Open Rotor Noise Impact on Airport Communities

PARTNER Project 35 Final Report

prepared by
Dimitri Mavris, Jimmy Tai, Russell Young, Ben Havrilesko

July 2011

Open Rotor Noise Impact on Airport Communities

PARTNER Project 35 Final Report

Dimitri Mavris, Jimmy Tai, Russell Young, Ben Havrilesko

PARTNER-COE-2011-007

July 2011

Project 35

Open Rotor Noise Impact on Airport Communities

Final Report

July 31, 2011

Principal Investigator: Dr. Dimitri N. Mavris (dimitri.mavris@ae.gatech.edu)
Co-Investigator/Institutional PI: Dr. Jimmy Tai (jimmy.tai@ae.gatech.edu)
Co-Investigator: Russell Young (russell.young@gtri.gatech.edu)
Co-Investigator/Graduate Research Assistant: Ben Havrilesko (benh@asdl.gatech.edu)

Aerospace Systems Design Laboratory
Guggenheim School of Aerospace Engineering
Georgia Institute of Technology
Atlanta, Georgia 30332-0150
Phone: 404-894-3343, Fax: 404-894-6596
Web: http://www.asdl.gatech.edu

Table of Contents

1.0 Project Overview

The highly tonal noise spectra produced by Open Rotor (OR) engines differ greatly from the relatively smooth, atonal noise spectra produced by typical Turbofan (TF) engines. Understanding the effects of these spectral differences on received noise is necessary for the prediction of the impact on community noise that this new engine may have. In this study, representative OR spectra were parametrically generated with characteristics and variations modeling those seen in the published OR data (Hoff 1990). With this generated range of representative spectra, two primary studies were performed. The first study examined the relationship between instantaneous noise metrics for representative TF and OR spectra while the second study explored the differences in noise contour area for representative TF and OR operations at equal certification levels.

Community noise predictions are typically focused on two areas, airport contours and certification. Certification is performed using the Effective Perceived Noise Level (EPNL) metric at three specific locations. This time dependent metric is derived from a time history of the instantaneous noise metric, Tone Corrected Perceived Noise Level (PNLT). Contours, however, use the Day Night Level (DNL) time dependent metric derived from the instantaneous metric of A-weighted sound pressure level (dBA). As PNLT includes a tone correction and dBA does not, it was anticipated that the drastically increased tonality of the OR spectra relative to the TF spectra could lead to an alteration of the relationship between these metrics. A variation in the relationship between the two instantaneous metrics could concurrently lead to a discrepancy in the relationship between community annoyance and certification levels. The first study sought to explore this possibility.

In order to perform the second study exploring contour differences between OR and TF operations at equal certification levels, it was necessary to calculate time dependent noise metrics. By applying propagation effects and Doppler shift to the representative spectra at discrete time steps of a trajectory for a stationary observer, a time history of noise was created for each stationary observer. The time history of noise was used to calculate duration corrected metrics at certification points and at a grid of observers to generate noise contours. Approximating the contour shape as an ellipse, contour area was estimated. By comparing OR contour area to the contour area of a typical 300 passenger class TF engine at equal certification levels, the effects of the spectral differences on community noise were explored.

2.0 Research Approach

2.1 Overview

The research efforts for Project 35 were performed over two years and may be logically broken down by the primary objectives for each year of the project. Several tools were developed and will be described in depth in the following sections. In the first year of the project, the primary objective was to compare instantaneous noise metrics for representative OR and TF spectra identifying any significant trends. Two tools were developed to achieve this goal. The first was used to calculate instantaneous noise metrics given input of one-third octave band spectra. By examining the OR spectra published by Hoff et. al (Hoff 1990) the characteristics of OR spectra were identified. The second tool employed a method developed for this project to generate spectra representative of noise emitted by a stationary OR engine

at full power using the characteristics observed in the Hoff data. Inputs for the tool were defined as parameters controlling the variation in the OR spectral characteristics observed in the published data. Approximately 3,000 representative OR spectra were generated by varying those parameters, and approximately 12,000 representative TF spectra were generated with the Environmental Design Space (EDS) program developed at Georgia Tech. The metric calculation tool was used to calculate metrics of interest for the OR and TF spectra.

In the second year of the project, the primary goal was to compare certification metrics and contours of TF and OR representative spectra. The metric calculation tool was expanded to allow for calculation of time dependent noise metrics. The OR representative spectra generation tool was modified to include the capability to predict time dependent changes to noise at a fixed observer through a full-power takeoff scenario. Then, a third code was developed to generate representative full-power takeoff trajectories with variation in Mach number and climb angle. Focusing on full-power takeoff scenarios, the stationary, full-power representative noise spectra were used as characteristic spectra to which propagation effects and Doppler shifting were applied throughout a representative takeoff. The noise was propagated at discrete time steps to stationary observers in order to generate a time history of the received noise at each observer location. Using this method, a time history of received noise was created for a grid of observers to generate a noise contour. In order to validate the time history generation method, a contour for a typical TF driven aircraft was generated, and the results were compared with those modeled by the NASA ANOPP L26v1.

Using the validated method of time history generation, the area of a given contour level was approximated using the following steps. First, the levels of each OR spectrum were normalized to result in a sideline (SL) effective perceived noise level (EPNL) equal to that of the TF contour used for validation. The SL noise is measured 1476 feet (450 m) from the runway centerline at a point where the noise level after liftoff is greatest. The SL normalization location was held constant regardless of trajectory changes, eliminating any contour differences associated with the changes in noise level of the generated spectra. Approximating the contour shape as an ellipse, as prescribed by Powell (Powell 2003), the vertices of the ellipse were found, and the area was estimated. The difference between the contour area of the OR and TF contours was calculated for a wide range of parametrically generated representative OR spectra.

2.2 Instantaneous Metric Comparison Approach

2.2.1 Metric Calculation Tool

The metric calculation tool was created in MATLAB version 7.8.0 (r2009a) and employed methods found in the literature to calculate the following metrics:

1. A-weighted SPL (dBA)
2. Tone Corrected A-weighted SPL (dBAT)
3. D-Weighted SPL (dBD)
4. Tone Corrected D-weighted SPL (dBDT)
5. Perceived Noise Level (PNL)
6. Tone Corrected Perceived Noise Level (PNLT)

7. Stevens' Perceived Noise Level (Mark VI)
8. Zwicker Loudness Level (Zwicker)
9. Overall Sound Pressure Level (OASPL)
10. Effective Perceived Noise Level (EPNL)
11. Sound Exposure Level (SEL)
12. Day-Night Average Sound Level (DNL)

As published work is available for a description of the methods to calculate the above metrics, such discussion will be sparse in this report. For exact details regarding formulation of these metrics, the reader is referred to the references. Here, we will discuss the integration of the metrics and the data required for their calculation by the tool.

Metric calculation begins with the input spectra. The generated tool accepts the input of tab or space delimited text files containing rows of one third octave band spectra from 50Hz to 10kHz. The first column is reserved for the discrete time value at which each spectrum occurs and is standardized to 0.5 second intervals. Columns two through twenty five contain the SPL of each third octave band. The 32 bit version of MATLAB is limited by a maximum variable size and a maximum memory usage of 2.14GB. Assuming a computer with enough RAM is used to run the tool, this MATLAB version can handle an input file containing 1×10^7 rows of spectra. In addition, the tool accepts multiple input files limited by the same maximum memory. Thus, the tool provides ample computational ability for our purposes.

Upon execution of the tool, the user is prompted in the MATLAB Command Window for all inputs required for calculation. The user enters each input filename and selects the metric or metrics to be calculated for each file. Each metric is calculated, and the results are presented in separate ASCII formatted text files containing a specific metric calculated for each spectrum in a single input file. For example, the output file 'Aweight1.txt' would contain the dBA values calculated for the spectra in the first input file.

The following description describes in more detail the individual metrics and modules that are present in the metric calculation tool created under this project.

Tone Correction Factor
The tone correction factor used for the A-weighted SPL, D-weighted SPL, and Perceived Noise Level calculations was calculated per the method outlined in the FAR 36 Appendix A2 (GPO Access, Electronic Code and Federal Regulations 2010). The tone correction factor was added to the final SPL calculated for the base metric to determine the tone corrected metric.

dBA and dBD
The A- and D-weighted SPL calculations were performed by calculating the A- or D-weighted level of each of the one third octave band frequency bins according to (ANOPP Theoretical Manual 2008) and performing a logarithmic summation of the full spectrum (Equation 1).

$$dBX = 10 \cdot log_{10} \left(\sum_{i=1}^{n} 10^{\frac{L_i}{10}} \right)$$

Equation 1

Here, L_i is the weighted level of the ith third octave band according to either the A- or D-weighting curve. The *X* in *dBX* represents the reference scale (*A* or *D* for A- and D-weighting respectively).

PNL, PNLT, and EPNL

Formulation of the PNL, PNLT and EPNL is outlined in the FAR 36 Appendix A2 (GPO Access, Electronic Code and Federal Regulations 2010). As each value was calculated using the preceding value (PNL→PNLT→EPNL), a single base module was used in the tool concluding at the appropriate level of the process to produce the requested metric. In order to handle the time dependent nature of the EPNL calculation, additional considerations were taken into account. Because several of the original test input files contained time dependent spectra from the cutback, sideline, and approach observer positions, it was necessary to determine the appropriate time intervals, should an input file contain multiple intervals requiring separate EPNL calculations. It was assumed in the generation of the tool that the concluding discrete time value for one interval would differ from the first discrete time value of the proceeding interval by more than 0.5 seconds. In this manner, the tool was designed to autonomously calculate the beginning and ending point of each time interval contained in the input file. As the end goal for this tool was to calculate metrics from spectra generated and manipulated by the author, it was sufficient to make this assumption.

Mark VI

The method for calculating Steven's loudness metric, Mark VI (calculated loudness level, S_P), was taken from the original publication of the method (Stevens 1961). Because much work was done in modifying this method for automated calculation, the formulation will be presented here.

The original documentation called for reference to a table and graph contained in the publication. Tabulated data was presented as loudness indices for discrete band pressure levels at 1000Hz. The graph showed a series of contours used to convert a level at a specific frequency band into the relative level at 1000Hz. In order to convert this into an automated method, the table was entered as a MATLAB matrix, and the graph was translated into a series of frequency and level dependant equations.

The graph depicted contours of constant loudness index depending on both band pressure level (dependent axis) and a logarithmic scale of frequency (independent axis). Contours on the graph followed lines of constant slope in three regions with two points of slope discontinuity. The first discontinuity was dependent on both band pressure level and frequency and followed a line having a continuous slope of -21dB/octave passing through the point (1000Hz, 10dB). The second discontinuity occurred at 9000Hz. Levels measured below the first line of discontinuity followed a line with a constant slope of -6dB/octave. Levels between the first and second discontinuities followed a line of a constant slope of -3 dB/octave. Above 9000Hz, contours had a slope of 12 dB/octave. A copy of this graph is shown in Figure 1 for clarification(Stevens 1961).
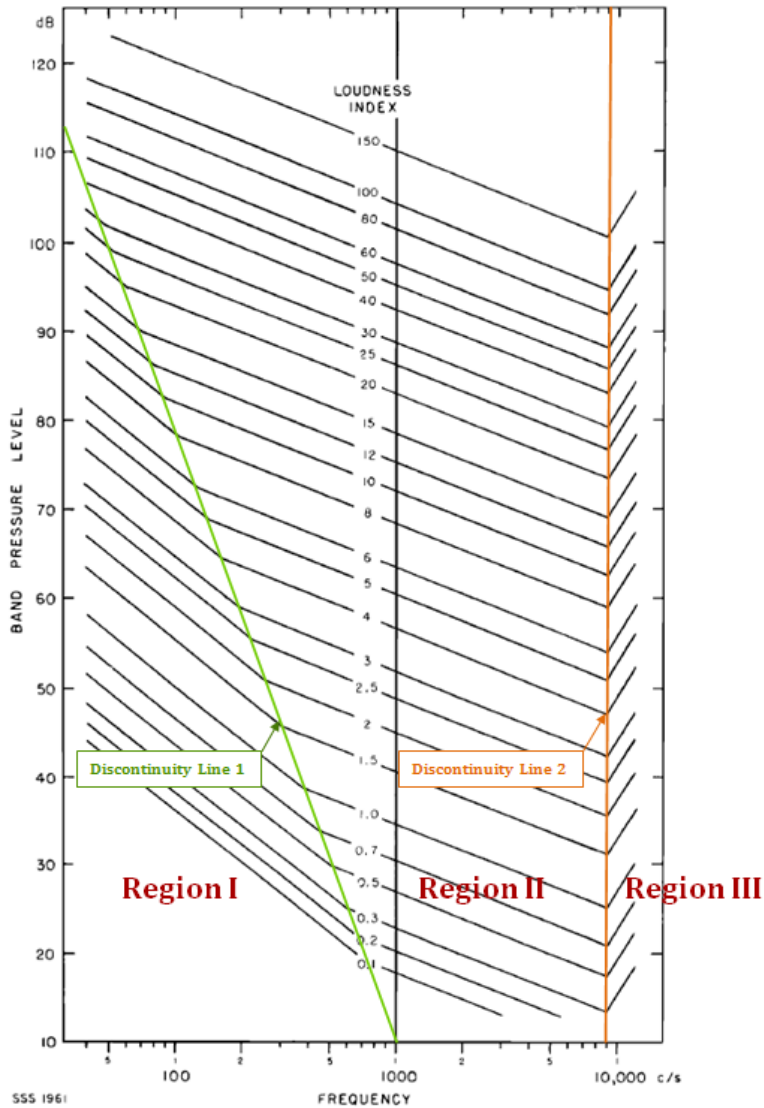
Figure 1: Stevens' Equal Loudness Diagram

In the following description of the methodology followed for generating the code to calculate Stevens' Loudness, we will consider a "point" to be a value of band pressure level and the corresponding band frequency. We will also denote three regions of interest in which a point may fall corresponding to the contour slope in that region and shown in Figure 1.

The end goal of this graph and table manipulation was to calculate the loudness index of a band pressure level at a given frequency by calculating the relative level at 1000Hz and then using the table to convert that level at 1000Hz to a loudness index. To do so, the generated code first determined the initial slope region of the given point. If the frequency of the point was below 1000Hz, it was necessary to determine if the point was located in Region I or Region II. This was done by the following steps: First, difference in frequency from the initial point to either 1000Hz, or the next point of slope discontinuity was converted to an octave value. This was required to use the octave dependent slope given by Stevens. To do so, Equation 2 was utilized:

5

$$dOct = log_2\left(\frac{f_f}{f_i}\right)$$

Equation 2

Where *dOct* was the number of octaves from the initial frequency, f_i, to the final frequency, f_f.

Next, the value of the discontinuity line at this frequency was calculated by Equation 3:

$$L_{discon} = \left(-21\frac{dB}{octave}\right)(dOct) + 10dB$$

Equation 3

Where f_f =1000Hz and f_i was the frequency of the point, f_o.

If this value was lower than the band pressure level of the point, the point was located in Region II and followed Equation 4 for calculation of the relative level at 1000Hz:

$$L_{1kHz} = L_o + \left(-3\frac{dB}{octave}\right)(dOct)$$

Equation 4

Where L_o was the band pressure level of the point and *dOct* was the number of octaves between the initial frequency and 1000Hz.

If the value of L_{discon} was higher than the initial band pressure level, the point was located in Region I. In this case, the point followed the slope of Region I until intersecting with the discontinuity line at a specified frequency, f_2, and then followed the Region II slope until reaching 1000Hz. To find the frequency of the point of discontinuity, a system of equations was solved. The process was as follows:

With reference to Figure 2, the equations for the lines F_1 and F_2 were given by Equation 5 and Equation 6:

$$F_1: \quad BPL_2 = BPL_1 - \left(6\frac{dB}{octave}\right) \times dOct_1$$

Equation 5

$$F_2: \quad BPL_3 = BPL_2 - \left(3\frac{dB}{octave}\right) \times dOct_2$$

Equation 6

6
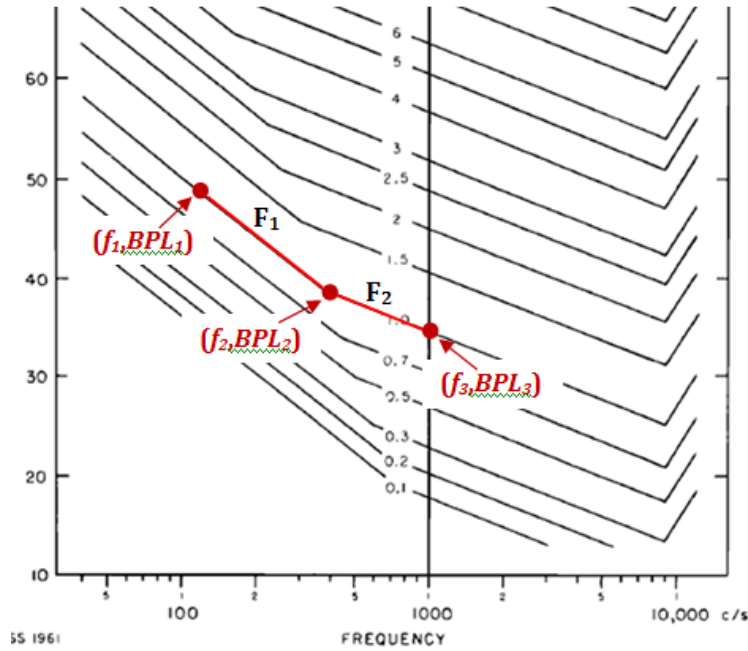
Figure 2: Stevens Equal Loudness Contour Diagram

In addition to these two equations, the equation for the line of discontinuity was employed and was given by Equation 7:

$$BPL_2 = 10dB + \left(21\frac{dB}{octave}\right) \times dOct_2$$

Equation 7

In Equation 5 through Equation 7, *dOct₁* and *dOct₂* are given by Equation 8 and Equation 9:

$$dOct_1 = log_2\left(\frac{f_2}{f_1}\right)$$

Equation 8

$$dOct_2 = log_2\left(\frac{f_3}{f_2}\right)$$

Equation 9

Combining Equation 5, Equation 7, Equation 8, and Equation 9 and simplifying gives:

$$log_2\left[\left(\frac{f_3}{f_2}\right)^{21} \times \left(\frac{f_2}{f_1}\right)^{6}\right] = BPL_1 - 10dB$$

Equation 10

Further simplification and isolation of f_2 along with utilization of the known value of $f_3 = 1000Hz$ gives Equation 11:

$$f_2 = \left[\frac{(1000Hz)^{21}}{(2^{BPL_1-10})(f_1{}^6)}\right]^{\frac{1}{15}}$$

Equation 11

With this value, the relative level at 1000Hz was calculated by Equation 12:

$$L_{1kHz} = L_o - \left(6\frac{dB}{octave}\right)dOct_1 - \left(3\frac{dB}{octave}\right)dOct_2$$

Equation 12

where $dOct_1$ and $dOct_2$ were the number of octaves between the initial frequency and f_2 and between f_2 and 1000Hz, respectively.

If the frequency was greater than 1000Hz but less than 9000Hz, the point lied in Region II, and Equation 13 was used to calculate the relative level at 1000Hz:

$$L_{1kHz} = L_o + \left(3\frac{dB}{octave}\right)(dOct)$$

Equation 13

where $dOct$ was the number octaves between the initial frequency and 1000Hz.

If the frequency was greater than 9000Hz, the point lied in Region III, and Equation 14 was used to calculate the relative level at 1000Hz:

$$L_{1kHz} = L_o - \left(12\frac{dB}{octave}\right)(dOct_1) + \left(3\frac{dB}{octave}\right)(dOct_2)$$

Equation 14

where $dOct_1$ and $dOct_2$ were the number of octaves between the initial frequency and 9000Hz and between 9000Hz and 1000Hz respectively.

8

With the relative level at 1000Hz known, the table was used to calculate the loudness index for each of the one third octave bands using linear interpolation for points lying between the given discrete values. The total loudness, S_t, in Sones was calculated by Stevens' formula given by Equation 15 (Stevens 1961):

$$S_t = S_m + F \left[\sum_{i=1}^{24} (S_i) - S_m \right]$$

Equation 15

where S_m was the maximum loudness index of the spectrum, F was a value given as 0.15 for spectra of one third octave bands, and S_i was the loudness index of the ith third octave band.

From the total loudness, the calculated loudness level, S_P, in Phons was determined by Equation 16 (Stevens 1961):

$$S_P = 2^{10(P-40)}$$

Equation 16

where (Stevens 1961):

$$P = 40 log_2 S_t$$

Equation 17

Zwicker

In order to calculate the Zwicker loudness level, a module previously written in MATLAB was adapted for use with our input spectra. The original module was based on the BASIC program published by Zwicker in 1991 (Hastings 2000) and took as an input 28 one third octave band levels for calculation while our data contained only contained 24 frequency bands. The module was modified following Zwicker's BASIC program formulation (Zwicker 1948) to accept our alternate input.

OASPL

The overall sound pressure level was given as the logarithmic sum of the band pressure level of each of the third octave bands by Equation 18 (ANOPP Theoretical Manual 2008):

$$OASPL = 10 log_{10} \sum_{i=1}^{24} 10^{\frac{L_i}{10}}$$

Equation 18

where L_i was the band pressure level of the ith third octave band.

2.2.2 Spectrum Generation Tool

In order to perform the study for Partner Project, it was necessary to explore a wide range of possible spectra likely to be produced by counter rotating open rotor systems. Though measured data has been gathered throughout the industry, the proprietary nature of this data made it impossible to procure for our study. If measured data was required and could not be garnered from outside sources, it would necessitate in house measurement of a wide range of CRP systems. The cost associated with such an undertaking proved far outside the scope of this study. Thus, it was necessary to artificially generate a range of spectra representative of the likely output of CRP systems. To do so, an initial program was generated to produce spectra with characteristics changing through the control of variables in the generation equations. This initial work was dispersed for industry feedback regarding the validity of the spectra generated. Feedback included reference to work published by G. E. Hoff et al. in 1990 (Hoff 1990) for comparison of the general attributes of CRP spectra. With this reference, the program was edited to include variables designed to capture the variability of the spectra published by Hoff. This work comprised the efforts in the first year of this project. In the second year of the project, modifications have been made to the spectra generation tool. The resulting spectra generation tool's variables and methodology will be discussed here along with the modifications made in year two.

In order to capture the dominating aspects of the variability exhibited by the various spectra published by Hoff (Hoff 1990), eight variables were considered for the initial time independent spectra characteristic of a stationary system. The eight initial variables used to generate the time independent spectra included:

1. Broadband Peak Frequency (BBF)
2. Broadband Peak Level (BBL)
3. Forward Propeller Blade Passing Frequency (BPF_f)
4. Aft Propeller Blade Passing Frequency (BPF_a)
5. Tone to Broadband Ratio (TTBB)
6. Forward Propeller Tone Scalar (TS_f)
7. Aft Propeller Tone Scalar (TS_a)
8. Specific Tone Scalar (TS_s)

The following illustration shows the effects of each variable on the resulting narrow band spectrum. This graphic is a rough qualitative representation of the variable effects and does not reflect exact dependence. In general terms, the variables were designed to have the following effects:

1. Broadband frequency and level determined the location of the peak of the broadband noise curve.
2. Blade passing frequencies determined the frequency of the initial tone and each subsequent tone.
3. Tone to broadband level determined the level of the primary tone relative to the broadband noise level.
4. Tone scalars determined the slope of the roll-off of the tones.
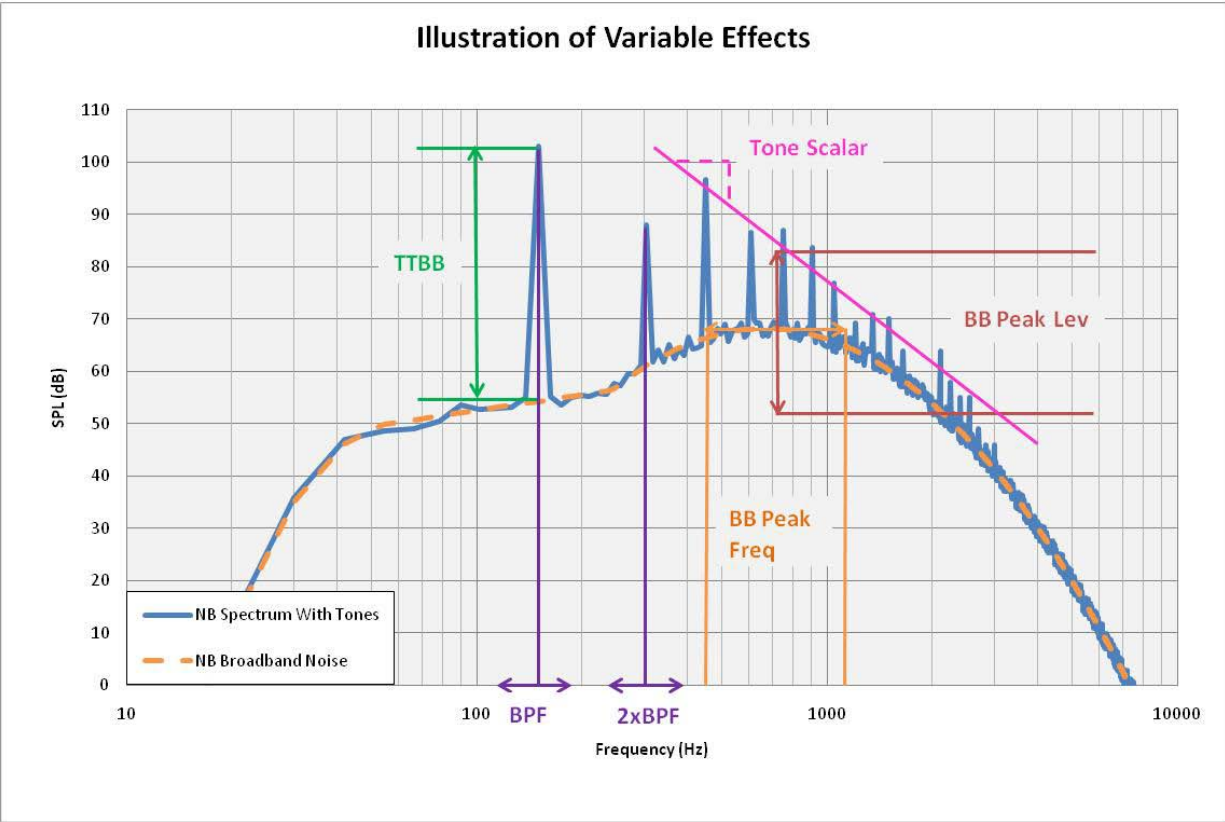
Figure 3: An Illustration of the Effects of Spectrum Generation Variables

A design of experiments was generated using these variables and an exploration of the ranges of these variables was performed.

*Note: All graphs in this section were generated using spectra generation method 2 as detailed below.

BBF and BBL

These two variables were used to determine the equation that would be used to govern the shape of the broadband noise. Based on the spectra published by Hoff et al., the broadband noise shape was approximated by a parabola on the logarithmic frequency scale with a modification made to the level at the frequency range before the peak of the parabola. The details of this equation are discussed in the Spectra Generation Tool Methodology section of this report.

The BBF variable was used to set the frequency at which the broadband noise parabola peaked in the 1/3 octave band graph. Similarly, the BBL variable was used to set the level of the peak of the parabola in the 1/3 octave band graph. Each variable had two settings, and the combination determined the coefficients to be used in the equation for the parabola predetermined for the four possible combinations shown in Figure 4 through Figure 7. BBF values of nominally 400Hz and 1000Hz and BBL values of nominally 65dB and 80dB were used for the broadband noise shapes. The setting of these variables controlled the shape by indirect manipulation, and expansion of the tool would require the generation of additional equation coefficients for the broadband parabola. The specific shapes were determined in order to most closely match data published by Hoff (Hoff 1990).

11
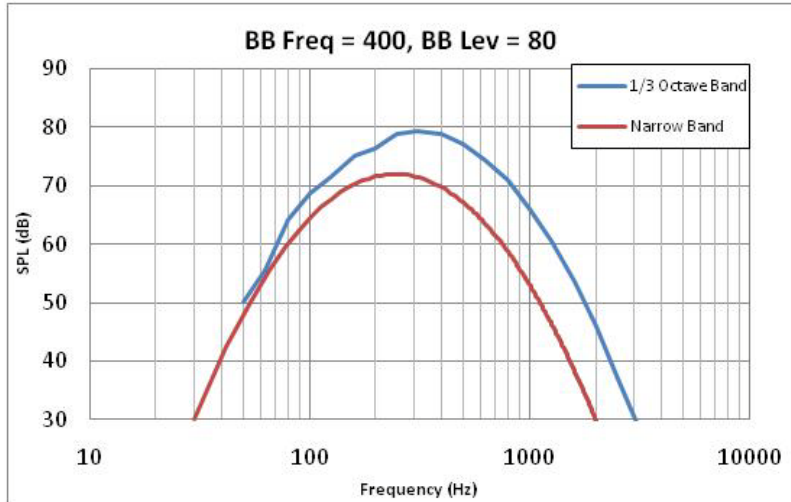
Figure 4: Narrow and 1/3rd OB Graph of Broadband Noise (BBF = 400 and BBL = 80)
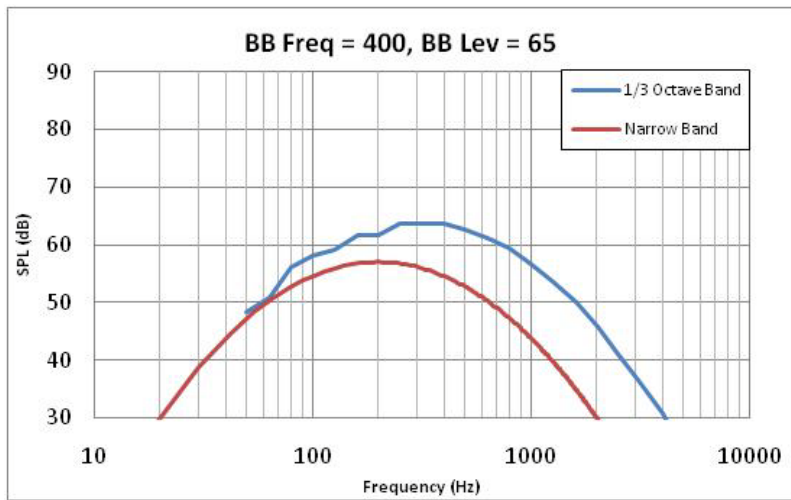
Figure 5: Narrow and 1/3rd OB Graph of Broadband Noise (BBF = 400 and BBL = 65)
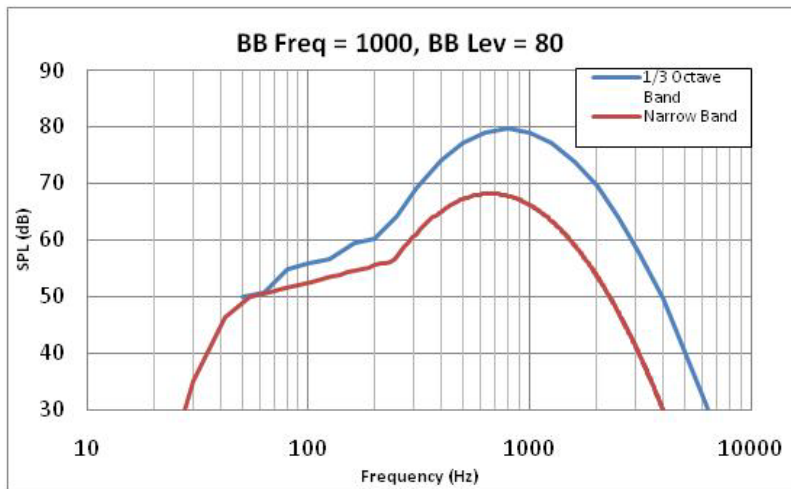
Figure 6: Narrow and 1/3rd OB Graph of Broadband Noise (BBF = 1000 and BBL = 80)

12
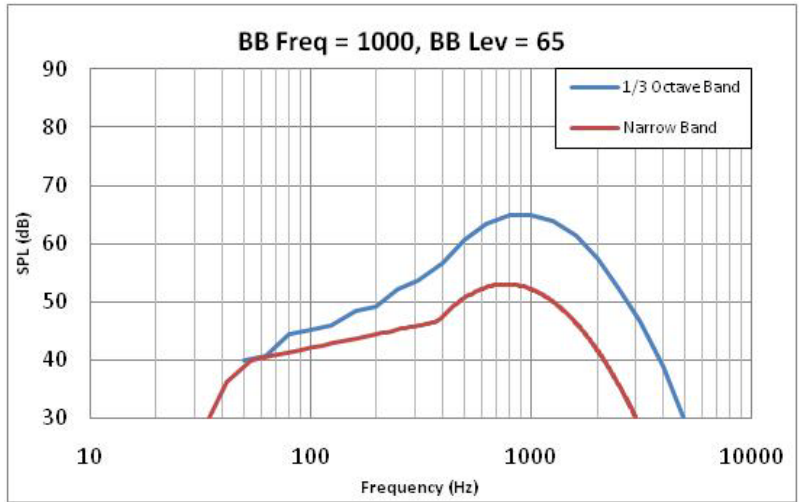
Figure 7: Narrow and 1/3rd OB Graph of Broadband Noise (BBF = 1000 and BBL = 65)

BPFf and BPFa

The BPF_f and BPF_a variables were used to set the blade passing frequency of the forward and aft propellers respectively. These values were used in the calculation of the frequencies at which tones were produced. For an nxn CRP where the BPF_f and BPF_a are equal, all tones occurred at a multiple of this frequency. Figure 8 shows an example where both BPF_f and BPF_a are set to 150Hz.

For an nxm CRP where the BPF_f and BPF_a are not equal, tones occurred at multiples of both frequencies, and interaction tones are introduced having frequencies of the sum of multiples of BPF_f and BPF_a (ex. $2 \times BPF_a + 3 \times BPF_f$). Figure 9 shows an example where BPF_f and BPF_a are set to 200Hz and 250Hz respectively. The range selected for this variable was 150Hz to 350Hz. The values were used directly in the calculation, and could thus be set at any value allowing for high flexibility of this aspect of the tool.
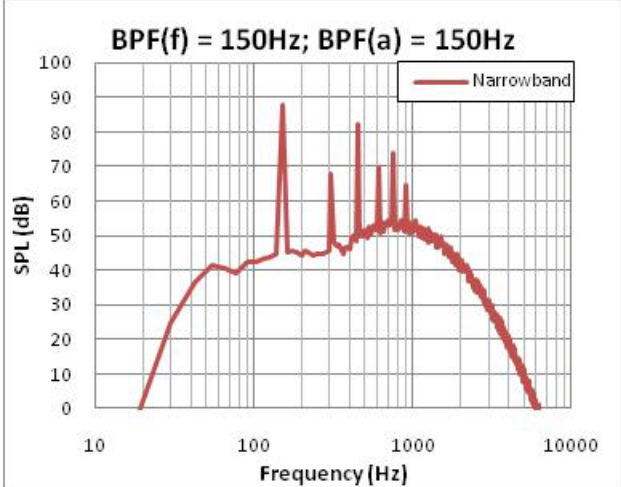
Figure 8: Effect of BPF for nxn CRP
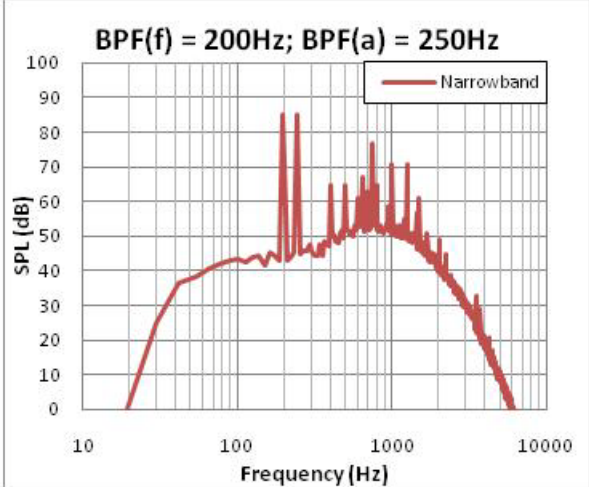
Figure 9: Effect of BPF for nxM CRP

13

TTBB

The variable TTBB determined the level of the tones generated in the narrowband relative to the broadband level at the given frequency. An increase in the variable increased the tone levels with respect to the broadband levels. Three settings were used: 10, 20 and 30. In Figure 10 and Figure 11, TTBB settings of 10 and 30 are shown respectively.
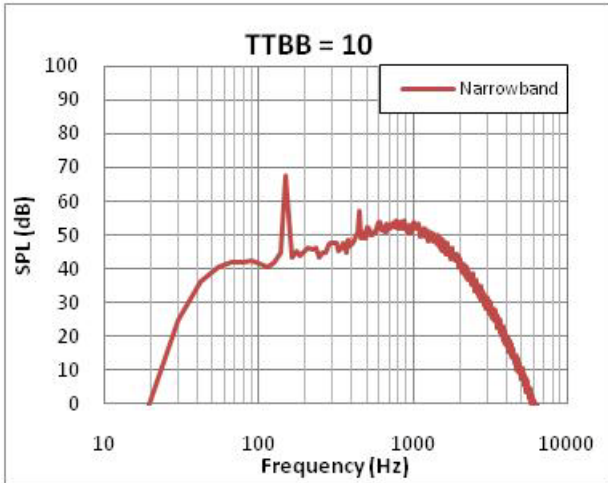
Figure 10: Effect of TTBB; TTBB = 10
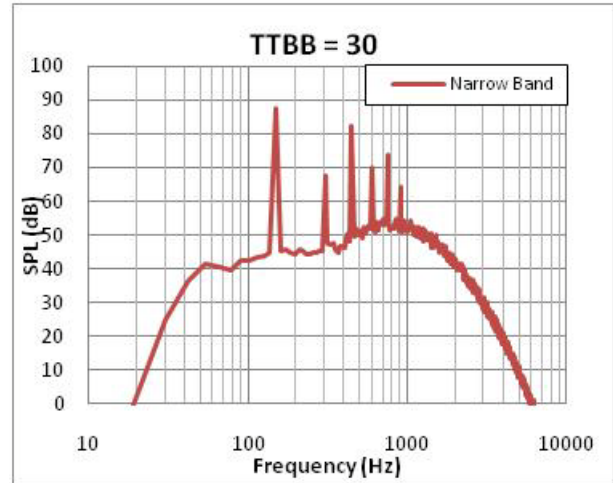
Figure 11: Effect of TTBB; TTBB = 30

TSf and TSa

The variables TS_f and TS_a allowed for further manipulation of the tone levels. With these variables, it was possible to allow for tones from either the forward or aft propeller to be more dominant. The variables also determined the general slope of the roll-off of tones. Figure 12 illustrates the effects of the tone scalar with each the TS_f and TS_a set to 1 and 2.
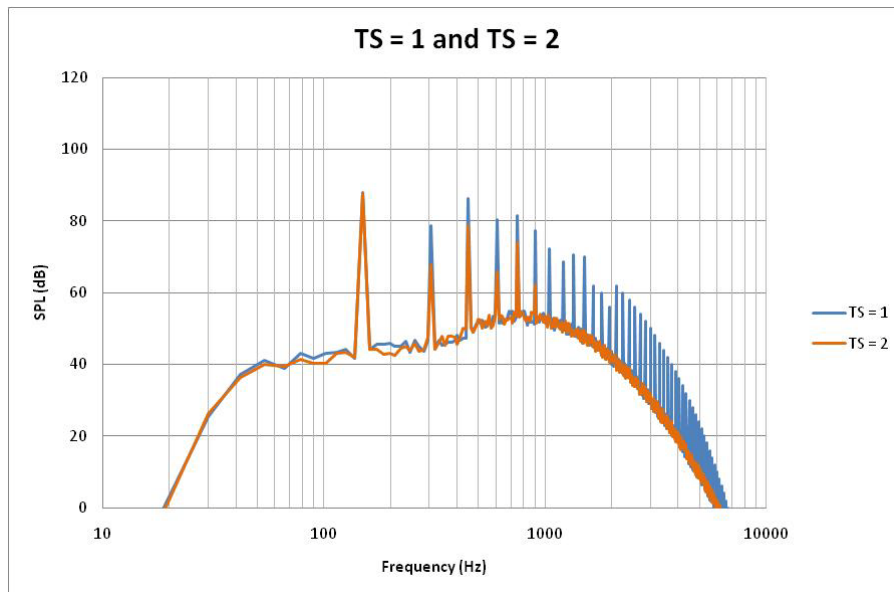
Figure 12: Effect of Tone Scalars; TS set to 1 and 2

14

<u>TSs</u>
The variable T_s was used to alter the levels of every third narrowband tone. This variable provided more variability in the tone levels relative to one another. An increase in this variable decreased the level of the tones to which it was applied.

2.2.3 Spectrum Generation Tool Methodology

The methodology followed by the spectra generation tool included two major iterations. In the first iteration (hereafter referred to as method 1), each tone level was defined relative to the broadband level at the frequency of the given tone and modified based on an attenuation value as detailed by McCurdy (D. A. McCurdy 1990). This method will be discussed in the first portion of this section. In the second iteration of the tool (method 2), the level of the initial "primary" tone manifesting at the blade passing frequency of the given propeller was defined based on the peak level of the broadband noise in the narrowband graph. Then, each subsequent tone was defined relative to the primary tone modified by the McCurdy attenuation value. All levels of tones preceding the primary tone depended only on the level of the primary tone. This modified method will be discussed in the second portion of this section.

<u>First Iteration</u>
In order to generate the initial spectra, the four major steps listed below were followed. Each of the steps is described in this section.

a. Calculation of broadband noise levels discretized into narrowband levels at 12Hz frequency intervals.
b. Calculation of narrowband steady-loading tone and interaction tone levels and frequencies.
c. Summation of tones into narrowband bins.
d. Summation of narrowband levels into one third octave bands.

The first step is to address broadband noise levels. As noted in the discussion of the BBF and BBL variables, the broadband noise levels followed four distinct predefined curves. The curves were generated using a MATLAB function that defined narrowband levels resulting in curves with one third octave band levels comparable to the curves observed in the spectra published by Hoff et al. (Hoff 1990). Along with the determined points for the appropriate peaks of the parabolas (ordered pairs of BBF and BBL), two points were observed from the Hoff spectra: the upper and lower frequencies at which the level dropped below 30dB. With these desired points for the one third octave band curves, the narrowband parabola equations were manipulated until each resulted in the desired one third octave band curve by altering the peak point and the two points at which the level fell below 30dB. The equation used followed the definition of a parabola with a substitution of variables generating the parabola on a logarithmic scale shown in Equation 19:

$$L_i = a[log(f_i)]^2 + b[log(f_i)] + c$$

Equation 19

where L_i is the level of the ith frequency, f_i, and a, b, and c were the coefficients to be determined.

With this equation, a system of equations was solved to find the coefficients a, b, and c using the three points discussed previously. It was discovered that this approach modeled well the cases in which the peak of the one third octave band curve occurred at 400Hz, but that it was difficult to achieve a representative curve with a peak at 1000Hz. Rather than add terms to Equation 19, thus increasing run time, the low frequency range of the narrowband curve was replaced by two curves: a line in the logarithmic scale following Equation 20, and a second parabola in the logarithmic scale following Equation 21. An illustration of the separate equations can be found in Figure 13.

$$L_i = m[log(f_i)] + n$$

Equation 20

where L_i is the level of the ith frequency, f_i, and m and n were constants to be determined.

$$L_i = a_2[log(f_i)]^2 + b_2[log(f_i)] + c_2$$

Equation 21

where L_i is the level of the ith frequency, f_i, and a_2, b_2, and c_2 were the coefficients to be determined.
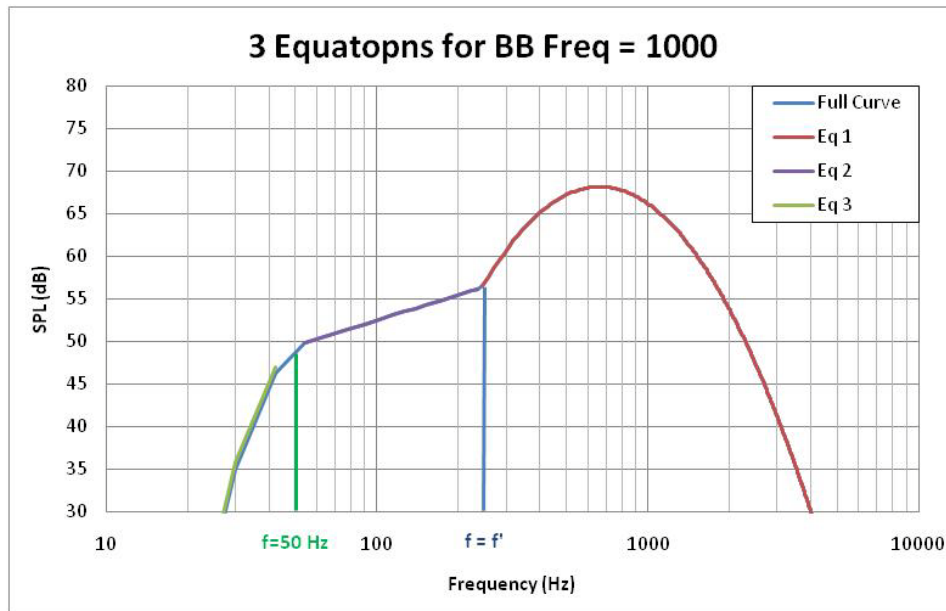
Figure 13: Illustration of 3 equations used in calculation of broadband noise

After coefficients a, b, and c were determined, the coefficient m was set to best model the slope of the low frequency region of the Hoff graphs, and the coefficient n was set to create an appropriate intercept

16

of Equation 20 and Equation 21 matching the levels observed in the Hoff data. This was repeated to find a_2, b_2, and c_2. This modification produced a better representation of the curves observed in the spectra published by Hoff et al., and can be seen in Figure 6 and Figure 7. For the broadband calculations of BB Peak set at 400, only Equation 19 was required (Figure 4 and Figure 6). For the broadband curves defined when BBF was set at 1000, the curves were governed by Equation 22:

$$L_i = \begin{cases} f < 50 & a_2[log(f_i)]^2 + b_2[log(f_i)] + c_2 \\ 50 < f < f' & m[log(f_i)] + n \\ f > f' & a[log(f_i)]^2 + b[log(f_i)] + c \end{cases}$$

Equation 22

The coefficients can be found in Table 1.

Table 1: Coefficients used in Broadband Noise Functions

BBF	BBL	a	b	c	a2	b2	c2	m	n
400	65	-27	124.25	-85.95	--	--	--	--	--
	80	-50.51	241.33	-216.27	--	--	--	--	--
1000	65	-66.55	384.53	-502.45	-146.97	532.56	-440.97	8	26
	80	-62.70	353.82	-431.02	-151.72	547.18	1442.21	10	32.5

With the values for the coefficients a, b, c, a_2, b_2, c_2, m, and n, the level of the broadband noise was calculated for each narrowband frequency bin with center frequencies from 6Hz to 11220Hz at 12Hz intervals. In order to model the random nature of the broadband noise, a randomized value from -2 to 2dB was added directly to the value of the broadband at each frequency (no logarithmic dB addition). The resulting randomized broadband noise may be seen in Figure 14. (Note that levels in the low frequency range appear less randomized because of the logarithmic axis.)
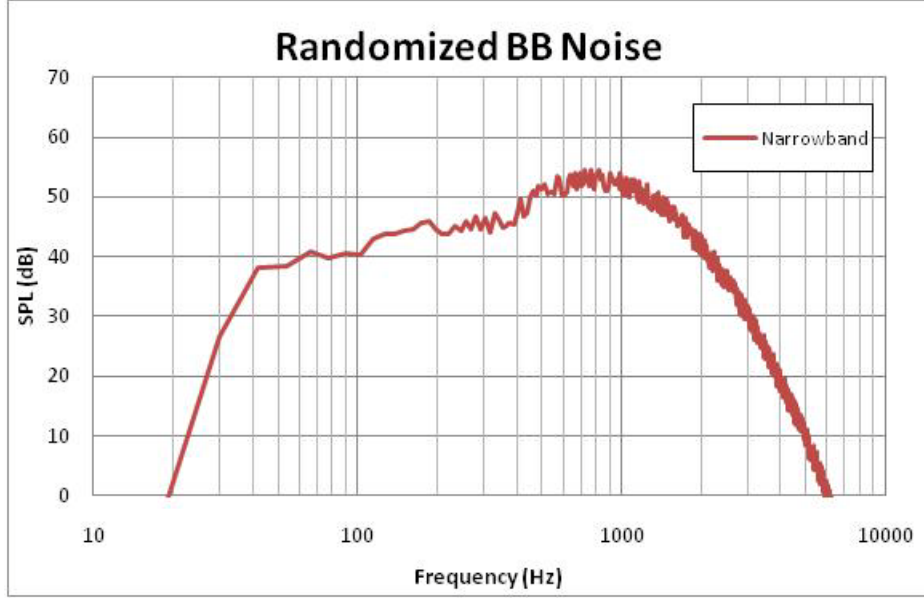
Figure 14: Plot of Broadband Noise with addition of Randomization

The next major step in generating the needed spectra is to address narrowband steady-loading and interaction tone-levels. Two types of tones were generated: steady-loading tones and interaction tones. Steady-loading tones represent the tones generated solely by the selected propeller. These tones were all integer multiples of the BPF of the given propeller. Interaction tones represent the tones generated by the acoustic interaction between the forward and aft propeller. For a given spectrum, each tone level and frequency was calculated and recorded before being sorted into bins. Both steady-loading and interaction tone levels were calculated following Equation 23:

$$L_{t,i} = L_{bb,i} + TTBB + M_n \times TS_p \times TS_s$$

Equation 23

where $L_{t,i}$ and $L_{bb,i}$ were the levels of the tone and the broadband noise at the ith frequency, respectively, *TTBB* was the tone to broadband ratio, TS_p was the tone scalar for either the forward or aft propeller, and TS_s was the specific tone scalar (TS_s was set to the given value for every third tone, and was set to 1 for every other tone).

For interaction tones, the tone scalar used was that of the highest multiple for BPF_a of BPF_f. For example, if the interaction tone occurred at $2 \times BPF_a + 3 \times BPF_f$, then the forward tone scalar was used. The value M_n was a relative peak value detailed by McCurdy for the nth tone (D. A. McCurdy 1990). The McCurdy relative peak value differed for steady-loading tones and interaction tones. The value was distinct for the specific multiples of the blade passing frequency of both the forward and aft propeller. Thus, the McCurdy relative peak value for the tone created by the second multiple of the forward propeller BPF and the third multiple of the aft propeller BPF ($2 \times BPF_a + 3 \times BPF_f$) differed from that of the tone created by the third multiple of the forward propeller BPF and the second multiple

18

of the aft propeller BPF ($3 \times BPF_a + 2 \times BPF_f$). A table of these values is provided in the appendix in Table 10.

The frequency at which a given steady-loading tone occurred was given by Equation 24:

$$f_{t,sl} = n \times BPF_p$$

Equation 24

where BPF_p was either the forward or aft blade passing frequency, and n was the tone number.

The frequency at which a given interaction tone occurred was given by Equation 25:

$$f_{t,int} = n_f \times BPF_f + n_a \times BPF_a$$

Equation 25

where BPF_f and BPF_a were the forward and aft blade passing frequencies, and n_f and n_a were the forward and aft tone numbers.

With tones created at multiples of both BPF_f and BPF_a as well as at the sum of multiples of BPF_f and BPF_a, it was possible for multiple tones to occur in the same narrowband frequency bin. Thus it was necessary to sum the levels by Equation 26:

$$L_{nb,i} = 10 log_{10} \left(\sum_{n=1}^{m} 10^{\frac{L_{i,n}}{10}} \right)$$

Equation 26

where $L_{i,n}$ is the nth tone in the ith frequency bin and $L_{nb,i}$ is the level of the ith narrowband frequency bin.

After this summation, the tone level at each frequency bin was compared to the broadband noise level. The greater of the two was passed on as the narrowband level at the given frequency.

The final step in the generation of time independent spectra required the summation of the levels of each narrowband frequency bin (either tone level or broadband noise level) into the appropriate one third octave band frequency bin. These values were summed according to Equation 27:

$$L_{i,1/3OB} = 10 log_{10} \left(\sum_{n=1}^{m} 10^{\frac{L_{i,nb}}{10}} \right)$$

Equation 27

19

Second Iteration
Although the method 1 resulted in spectra closely matching those presented by Hoff, it was determined that the method could be improved. The tone levels defined in method 1 depended both on the broadband level at the tone frequency and the McCurdy attenuation factor for the tone number. In examining the resulting spectra garnered from method 1, it was found that the primary tone in the 1/3 octave band graph often did not have the highest level (Figure 16). This phenomenon did not follow any of the representative spectra observed in the literature (Figure 15: (D. A. McCurdy 1990)), thus it was determined that method 1 could be modified to even more closely match the published spectra by altering the definition of the tone levels.

McCurdy's experimental attenuation factors were defined relative only to the primary tone level. In the second iteration, method 2, the primary tone level was defined relative to the broadband shape, and all subsequent tone levels were defined relative to the primary tone using only McCurdy's attenuation factors. This altered methodology will be discussed first. Due to the adjusted attenuation, high frequency tones showed much less roll-off. In order to achieve the desired attenuation at high frequencies, the tone scalar ranges were altered. This alteration will be discussed in the second portion of this section.
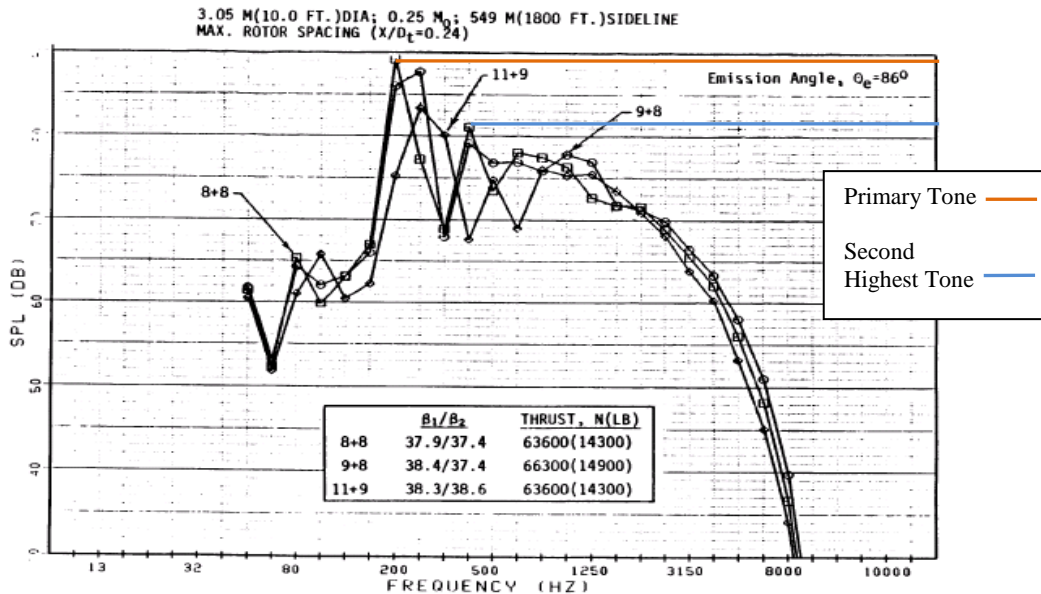
Figure 238. Spectra of F-7/A-7 with Different Blade Numbers at Typical Takeoff Thrust.

Figure 15: Graph of Representative spectra Illustrating relative tone levels (Hoff 1990)
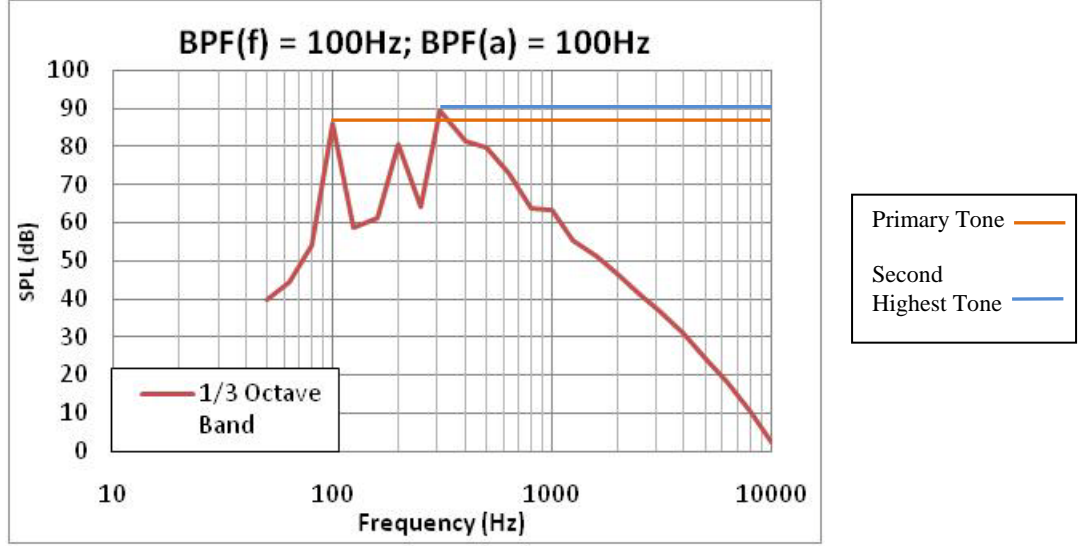
Figure 16: Graph of Method 1 Spectra Illustrating Relative Tone Levels

The steps for method 2 differ from method 1 only in step 2, the calculation of narrowband steady-loading tone and interaction tone levels. First, the primary tone level was defined relative to the given broadband shape in the narrowband graph. It was discovered that for low frequency BPFs if the primary tone level was defined relative to the broadband level at the BPF, the tone may be exceedingly low, and possibly even lower than the peak of the broadband. To adjust for the possibility of a range of blade passing frequencies, the primary tone was defined relative to the maximum level of the broadband noise at the BPF. During the generation of the broadband noise levels in narrowband, the maximum value was stored for use in this calculation. The primary tone level was set according to Equation 28.

$$L_{t,p} = L_{bb,max} + TTBB$$

Equation 28

where $L_{t,p}$ the primary tone level, $L_{bb,max}$ was the maximum level of the given broadband shape, snd *TTBB* was the tone to broadband setting for the run.

This level was set for the primary tones generated by both the fore and aft propellers, and all subsequent tone levels (both steady-loading and interaction) were set relative to this level as dictated by Equation 29.

$$L_{t,i} = L_{t,p} + M_n \times TS_p \times TS_s$$

Equation 29

where $L_{t,i}$ was the ith tone level, $L_{t,p}$ was the level of the primary tone, M_n was the McCurdy relative attenuation value the nth tone, TS_p was the tone scalar for either the forward or aft propeller, and TS_s was the specific tone scalar (TS_s was set to the given value for every third tone, and was set to 1 for every other tone).

21

As in method 1, the tone scalar used for interaction tones was that of the highest multiple for BPF_a of BPF_f. Further steps in the spectra generation following method 2 were identical to steps 3 and 4 of method 1.

Spectra generated using method 2 achieved the desired relative tone levels for the lower tone numbers, and the general shape in the lower frequency range matched the published data. However, the roll-off at higher frequencies did not follow the observed results from the published data. With only the attenuation factor detailed by McCurdy, tones appeared at relatively high levels at very high frequencies. Furthermore, high tone density occurred in high frequency 1/3 octave band bins. This increasing density comes from manifests because with increasing frequency, the range of each 1/3 octave band bin increases. Tones occur at integral multiples of both propeller BPFs (steady-loading tones) and at the sum of integral multiples of the two propeller BPFs (interaction tones, ex. $2xBPF_f + 4xBPF_a$). Thus, tone frequencies increase linearly while frequency bin ranges increase logarithmically. The relatively high tone levels and the high tone density at high frequencies resulted in essentially and increased flat broadband noise in the high frequency range (Figure 17).

It was determined that this representation was not consistent either in narrowband or in 1/3 octave band with the published data. In order to correct this, the tone scalar range was adjusted to increase the attenuation. As McCurdy's attenuation factor increased in magnitude at an approximately linear slope, the tone scalar increase effectively increased the magnitude of the slope. Thus the lower frequency attenuation increase was less than the increase in attenuation at the high frequency. This served to preserve the low frequency data that was previously determined to be consistent with published data. The resulting spectra showed a more reasonable roll-off and produced 1/3 octave band graphs consistent with published data (Figure 18).
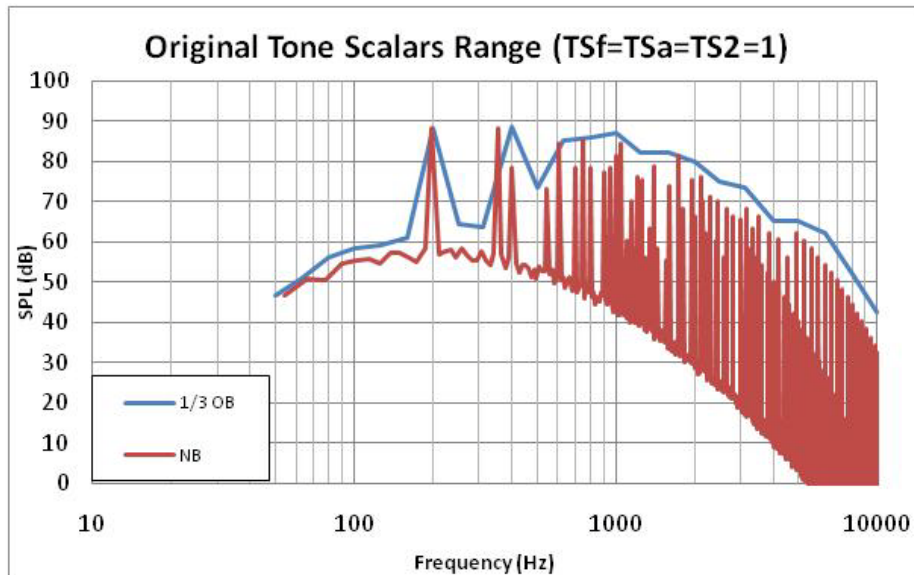
Figure 17: Tone Scalars set to 1 with Method 2 Tone Definition Logic

22
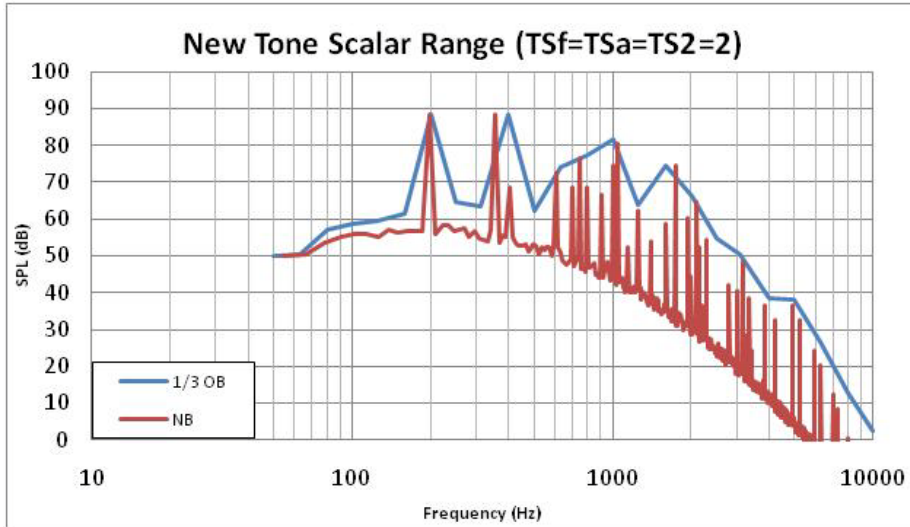
Figure 18: Tone Scalars Set to 2 with Method 2 Tone level Definition Logic

2.3 Contour Comparison Approach

2.3.1 Parametric Trajectory Generation

To study the effects of the flight path on the OR contour area, a series of flight paths were generated parametrically. The flight paths originated at a constant lift-off point 5000 feet down-field of the brake release point on the runway center line. The Mach number, climb angle, and angle of attack were held constant through a given trajectory to generate x- and z-coordinates of the aircraft location at 0.5 second time steps. Using the standard atmosphere model from ANOPP, the speed of sound and ambient density were calculated based on the altitude at each time step. To generated varied flight paths, the Mach number and climb angle were varied for each case. Figure 19 shows the parametrically generated flight paths compared with the flight path flown by the representative TF driven aircraft which was generated using NASA's Flight Optimization System (FLOPS) program.
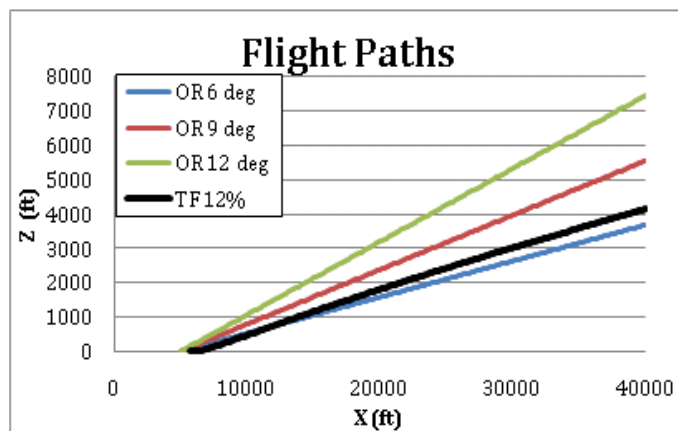
Figure 19: Parametrically Generated Flight Path

23

2.3.2 OR Time History Generation

In order to model a realistic time history of the noise received at a stationary observer location, several effects were applied to the representative stationary, full-power noise spectra including:

    i.   Doppler shift
    ii.   Directivity attenuation
    iii.   Spherical spreading
    iv.   Atmospheric attenuation

<u>Doppler Shift</u>
The Doppler shift is a change in frequency of a wave for an observer when relative motion exists between the source and observer. The high speed of an aircraft is enough to cause a drastic frequency shift. As human perception of sound is highly frequency dependent, this shift can have a significant effect on annoyance.

For the application of the Doppler shift, it was assumed that the aircraft followed a two-dimensional, takeoff trajectory with variation in altitude and in the distance traveled in the direction parallel to the runway. Using the two dimensional velocity and position data at each time step, the velocity of the aircraft relative to the observer was calculated. The equation for calculating the new frequency altered due to the Doppler shift is given in Equation 30 (Kinsler, et al. 1999):

$$f_D = f_o \left(\frac{c + v_r}{c + v_s} \right)$$

Equation 30

Here, f_o was the initial frequency, c was the speed of sound in the medium, v_r was the velocity of the receiver with respect to the source, and v_s was the velocity of the source with respect to the receiver. For our assumptions, the receiver was stationary ($v_r = 0$) and the source had a velocity with only x and z components.

Figure 20 shows the representation of the vector $\vec{r}$ giving the position of the aircraft with respect to the observer. The y component is not shown as there was no change in this y-position relative to the observer throughout the trajectory. In order to calculate the velocity of the source with respect to the receiver, the change in the magnitude of $\vec{r}$ was found with reference to Figure 20, by Equation 31:

$$v_s = \frac{d|\vec{r}|}{dt}$$

Equation 31

Here, $|\vec{r}|$ was given by:

$$|\vec{r}| = \sqrt{(x_o + v_x t)^2 + (y_o)^2 + (z_o + v_z t)^2}$$

Equation 32

Here, x_o, y_o, and z_o were the x-, y-, and z-distance from the aircraft to the receiver respectively at the beginning of the given time step, v_x and v_z were the horizontal and vertical components of the velocity of the aircraft, and t was the time. Differentiating Equation 32 with respect to t gave:

$$\frac{d|\vec{r}|}{dt} = v_s = \frac{(x_o + v_x t)v_x + (z_o + v_z t)v_z}{\sqrt{(x_o + v_x t)^2 + (y_o)^2 + (z_o + v_z t)^2}}$$

Equation 33
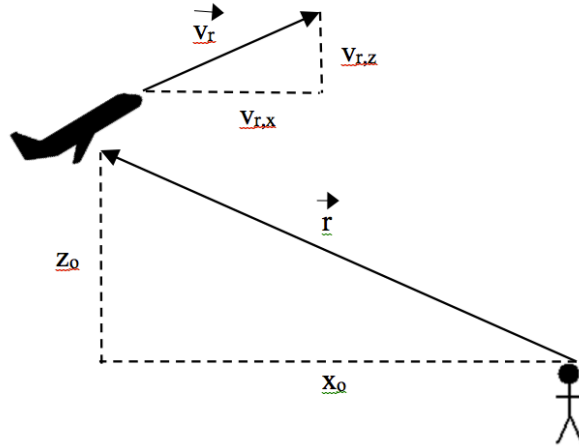
Figure 20: Illustration of the Motion of the Aircraft with Respect to the Receiver

The values for the initial position and velocity variables in Equation 33 were given for each time step by the discretized trajectory. As each time step had a time increment of 0.5 seconds, the value for t in Equation 33 was always 0.5 seconds. The value calculated here for the velocity of the aircraft with respect to the observer was substituted into Equation 30, and was applied to each tone calculated for the stationary spectrum in the narrowband.

Directivity Attenuation
For the OR directivity pattern, a simplified pattern was borrowed from McCurdy (D. A. McCurdy 1990) and can be seen in Figure 21. This plot shows the change in attenuation of the emitted sound as the directivity angle deviates from the engine axis. Here, it is assumed that this attenuation is constant across all frequencies and 360 degrees about the engine axis.

To find the directivity angle, the position data from the trajectory was used. Referencing Figure 20, the cosine of the directivity angle was found from the dot product of the position vector, $\vec{r}$, and the velocity vector, $\vec{v_r}$, and the directivity angle was found by Equation 34:

$$\theta_d = \cos^{-1}\left[\left(\frac{\vec{r}}{\|\vec{r}\|}\right) \cdot \left(\frac{\vec{v_r}}{\|\vec{v_r}\|}\right)\right]$$

Equation 34

Here, θ_d is the directivity angle. Figure 21was discretized using a digitization program, and linear interpolation was used to determine the attenuation at the given directivity angle.
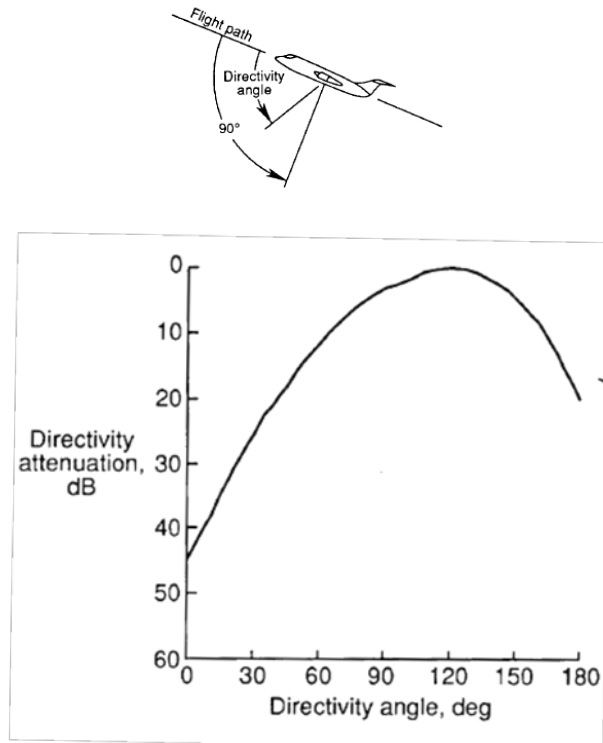
Figure 21: McCurdy Directivity Attenuation (3)

Spherical spreading
For the calculation of the effect of spherical spreading, the distance from the observer to the aircraft was calculated. This was given by the magnitude of the position vector, $\vec{r}$, as given by Equation 32. With the distance between the observer and the aircraft, the attenuation due to spherical spreading was given by Equation 35:

$$L = 20log_{10}\left(\frac{r_{ref}}{|\vec{r}|}\right)$$

Equation 35

Here, L was the attenuation in dB that was added to the initial level and r_{ref} was the reference distance. The generated spectra were representative of the Hoff (Hoff 1990) data referenced to 1800 feet. Thus the reference distance for all generated representative spectra was given to be 1800 feet.

Atmospheric attenuation
For the calculation of the noise level reduction due to atmospheric absorption, a model was used based on a model found in Kinsler (Kinsler, et al. 1999). The model assumed a constant temperature and humidity through the relatively low altitude variation of the takeoff. For our purposes, one-third octave band resolution was used in the application of the frequency dependence of the absorption.

26

Given humidity and frequency, the absorption model provided the attenuation in units of decibels per meter. Multiplying this value by the distance from the aircraft to the observer (given by Equation 32) gave the attenuation for each one-third octave band.

2.3.3 Metric Calculations and Contour Generation

Applying each of the above effects resulted in an instantaneous noise spectrum received by the observer for each time step in the trajectory. With this time history of the received noise, duration corrected metrics could be calculated. A time history was generated for the SL certification observer point and for a grid of stationary observer points to generate a noise contour. The EPNL was calculated for each observer location. This metric was chosen as it is the standard for aircraft certification outlined by FAR 36 (GPO Access, Electronic Code and Federal Regulations 2010).

Observer Locations
For proper comparison to the TF contour, the levels of the characteristic OR spectra used to generate the time history were modified in level such that the resulting contour would have an EPNL equal to that of the TF contour at the SL observer. A value was added to each of the one-third octave band levels in the OR spectrum. Using the Golden Section optimization method (Vanderplaats 2007), this value was optimized to minimize the difference between the OR SL EPNL and the TF SL EPNL. The normalized OR spectrum was then used as the characteristic spectrum to generate the time history for each point in the observer grid.

The EPNL at each grid location was calculated based on the time history of received noise. The EPNL was calculated for observers at one side of the runway center line and reflected about that line to generate contours. The contour levels ranged from 80 dB EPNL to 110 dB EPNL at 5 dB EPNL increments. Further discussion and examples of generated contours may be found in the Results and Analysis section.

OR Contour Generation
A grid of observer positions (observer grid) was generated for initial screening with 500 feet intervals in the direction perpendicular to the runway (y-direction), and 1500 feet intervals in the direction parallel to the runway (x-direction). In order to eliminate error in assumptions and unaccounted effects during ground roll, the grid originated at the 10,000 feet (5,000 feet down-field of the lift-off point). To decrease run time, it was assumed that the contour was symmetric about the runway, and points on only one side of the runway center line were calculated.

TF Contour Generation
Because the directivity of the noise generated by a TF engine is quite complex, a simple directivity angle level attenuation, such as that used for the OR contour generation, resulted in a poor match to the ANOPP calculation. To better model this complex directivity, ANOPP was manipulated to generate a characteristic TF spectrum for directivity angles from -10 to 190 degrees from the polar axis at 1 degree increments. Observers were set in a 100 feet radius arc as seen in Figure 22, and the aircraft was flown at very low velocity along a flight path passing through the center of the arc. Spectra were gathered for

each observer location at the point when the aircraft was at the center of the arc to generate a directivity model for the TF driven aircraft.
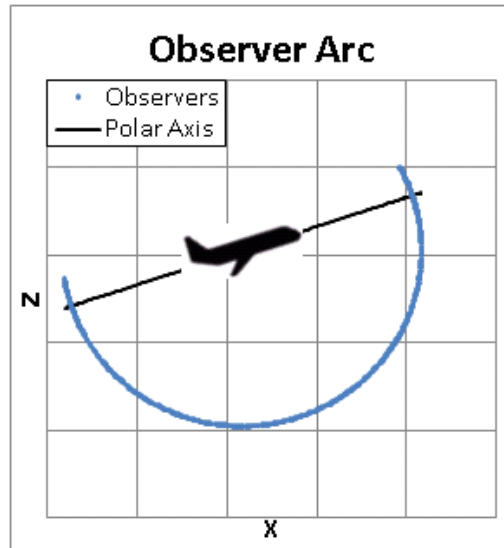
Figure 22: TF Directivity Arc

In the generation of the time history, the directivity angle was calculated as the dot product of the position and velocity vectors as in the OR method. For a given directivity angle between the observer and the engine polar axis, the spectrum generated by ANOPP at that angle in the observer arc was used as the characteristic spectrum to which propagation effects were applied. For angles between the 1 degree steps, the spectrum of the closest angle was used. In every manner except the directivity, the OR and TF time history generation methods were identical.

2.3.4 Contour Area Calculation

To determine the area of a given contour level, the contour shape was approximated by an ellipse. Because our method does not model noise from ground roll, the area calculation was limited to observers at x-locations greater than or equal to 10,000 feet from the brake release point. The calculation of the area of the contour ellipse required definition of the major and minor vertex locations.

X-direction Vertex
Because all flight paths were known to be along the runway center line, the vertex in the x-direction was assumed to lie on the runway center line. For an input contour level, the vertex location finder stepped with an initial step size out from 10,000 feet in the x-direction until the EPNL was below the input level. The step size was decreased upon calculation of an EPNL lower than the input level, and the search resumed. This was iterated until the step size reached a minimum value. For the results presented in this report, the minimum step size was 200 feet, providing a predicted x-direction vertex location ($x_{xvert,p}$) accurate to $x_{xvert,p} \leq x_{xvert,actual} < x_{xvert,p}+200$ feet.

Y-direction Vertex

28

Calculation of the location of the y-direction vertex required finding both the x- and y-locations ($x_{yvert,p}$ and $y_{yvert,p}$). Here, because the flight path was smooth, it was assumed that there would be only one maximum along the full x-range for a given value of y. With this assumption, the Golden Section optimization method was used to find the maximum EPNL at a given y value. If this maximum was greater than the desired contour level, the y value was increased by a given step. If the maximum was less than the desired level, the y-step was decreased. This was iterated until a minimum y-step was reached. The value of $x_{yvert,p}$ was taken to be the last maximum from the Golden Section optimization above the desired level and $y_{yvert,p}$ was taken to be the y value at which the last maximum above the desired level occurred. For our results, the minimum step was again 200 feet, and the Golden Section optimization was performed to a tolerance of 200 feet.

With the coordinates of the vertices determined, the lengths of the major and minor vertices of the contour ellipse were calculated by the following equations:

$$a = x_{xvert,p} - x_{yvert,p}$$

Equation 36

$$b = y_{yvert,p}$$

Equation 37

The y-vertex was nearly always located past the 10,000 feet contour area cut-off. To calculate the portion of the contour ellipse past 10,000 feet, the following equation was used:

$$A = a \times b \times \left(\frac{\pi}{2} + \sin^{-1}\left(\frac{c}{a}\right)\right) + b \times c \times \frac{\sqrt{a^2 - c^2}}{a}$$

Equation 38

Here, c is the distance from the vertex to the 10,000 feet cut-off calculated by:

$$c = x_{yvert,p} - 10,000ft$$

Equation 39

Figure 23 illustrates each of the values in Equation 36 through Equation 39.
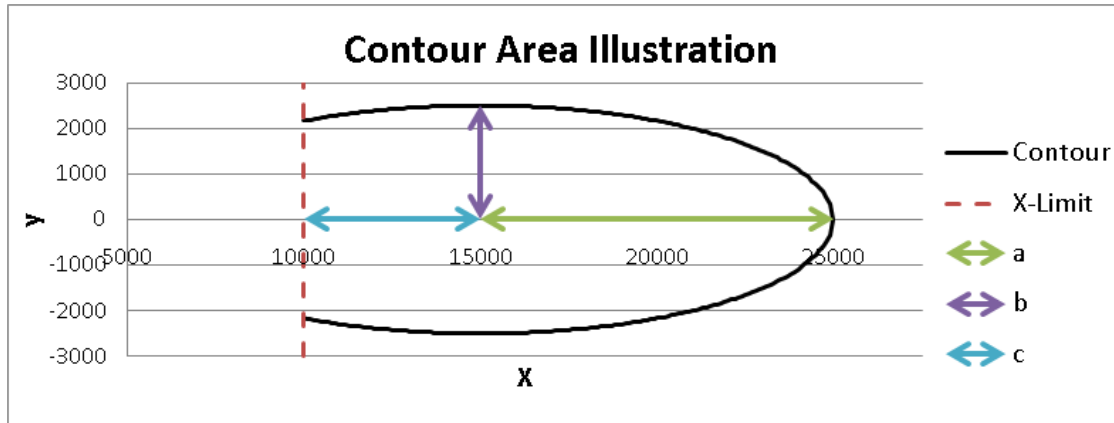
Figure 23: Contour Area Illustration

3.0 Results and Analysis

The results of Project 35 are broken down into two sections. First, the results of the instantaneous metric study are presented, and then the results of the time dependent metrics are presented.

3.1 Instantaneous Metric Relationships

Results for the instantaneous metric study were published in June of 2010. Further examination of these results led to a second iteration of the spectrum generation method. A series of spectra are presented below comparing method 1 results to method 2 results given the same input parameters. After determining that the second iteration of the spectrum generation method produced more representative spectra as compared to the Hoff data (Hoff 1990), the results were revisited. Applying the improved spectrum generation method, the results were reproduced, and the findings are presented below.
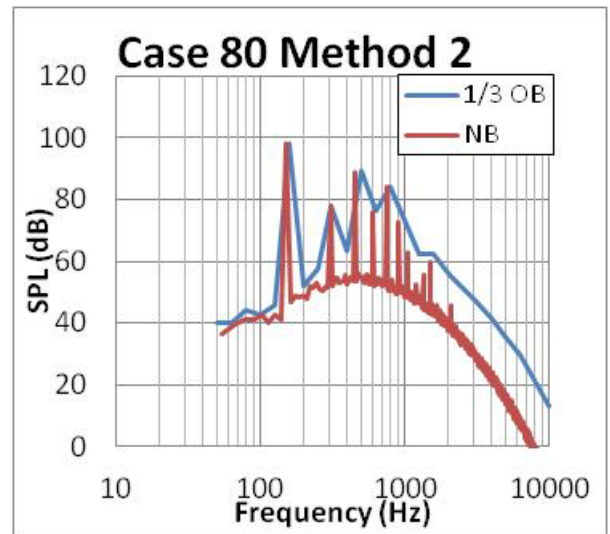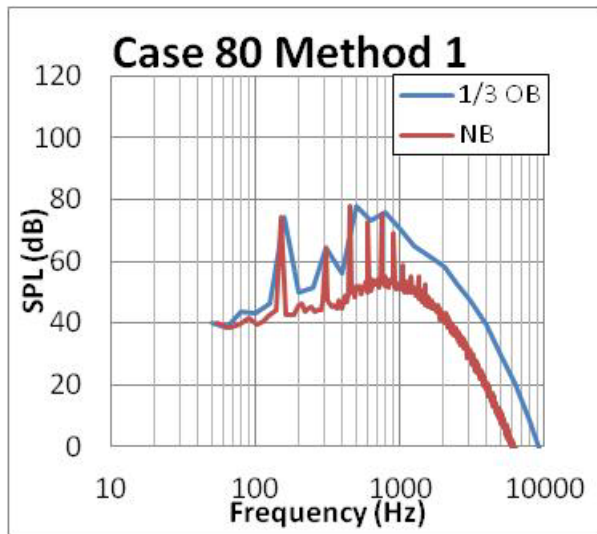
Figure 24: Spectra Comparison for Case 80
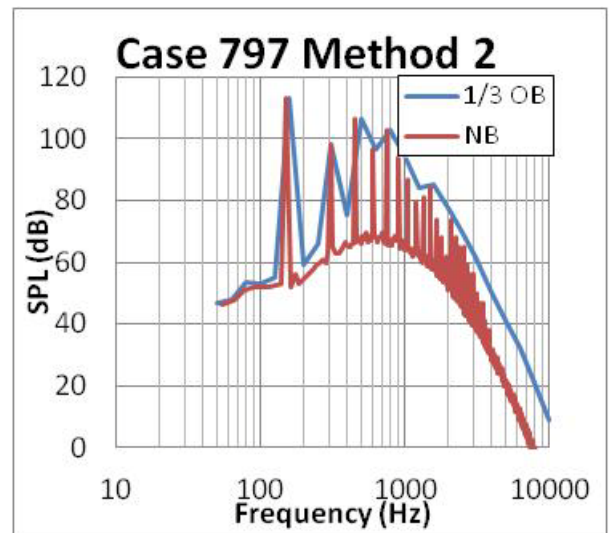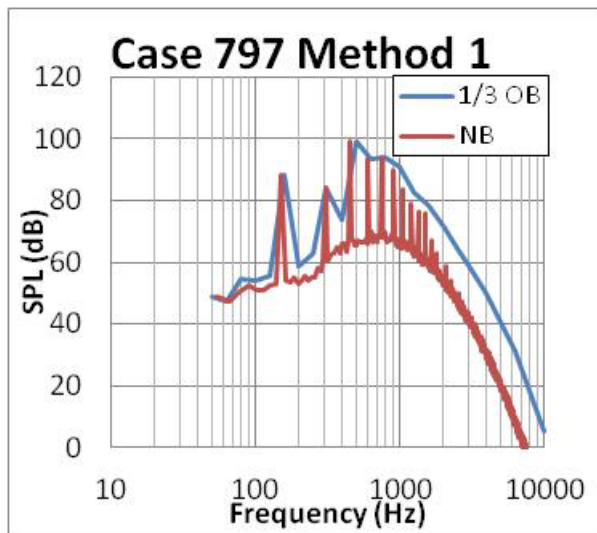
Figure 25: Spectra Comparison for Case 797
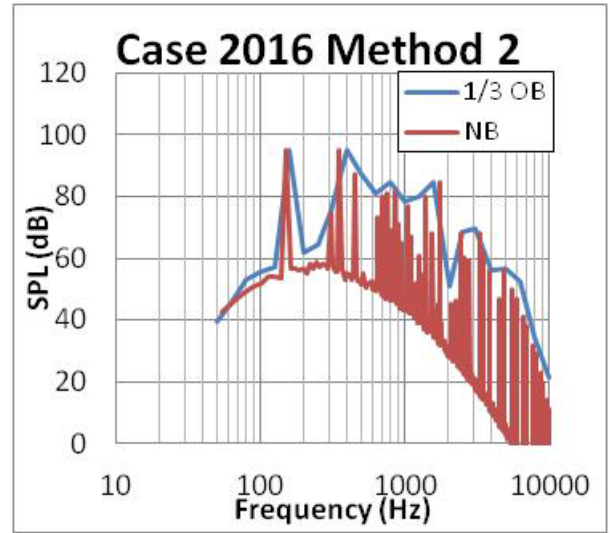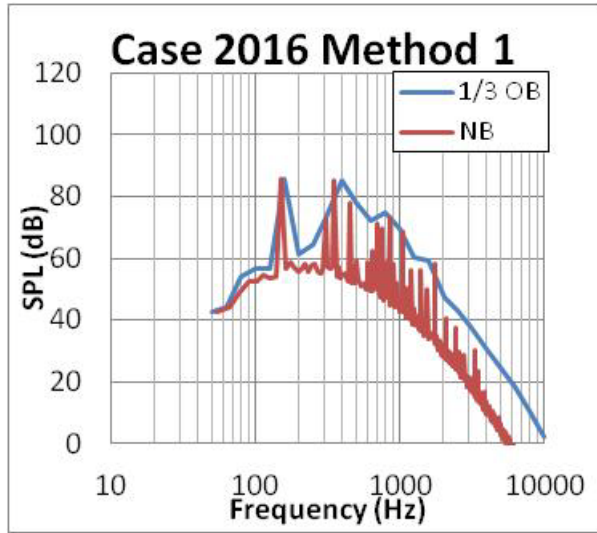
Figure 26: Spectra Comparison for Case 2016
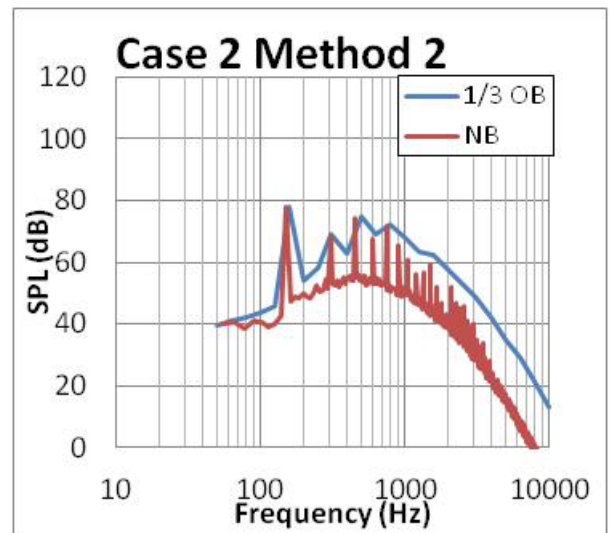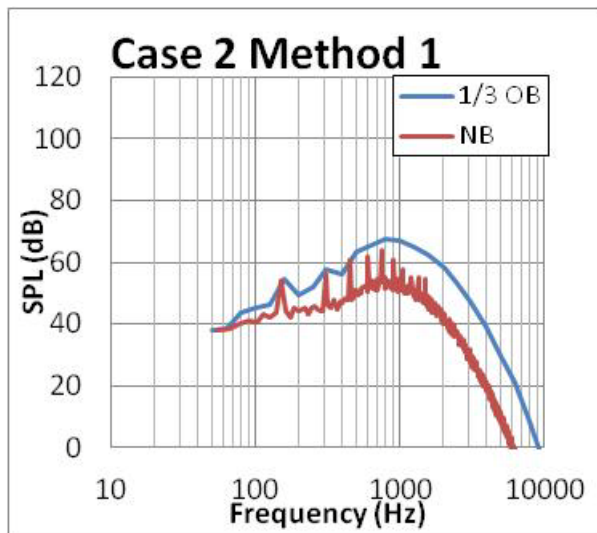
Figure 27: Spectra Comparison for Case 2
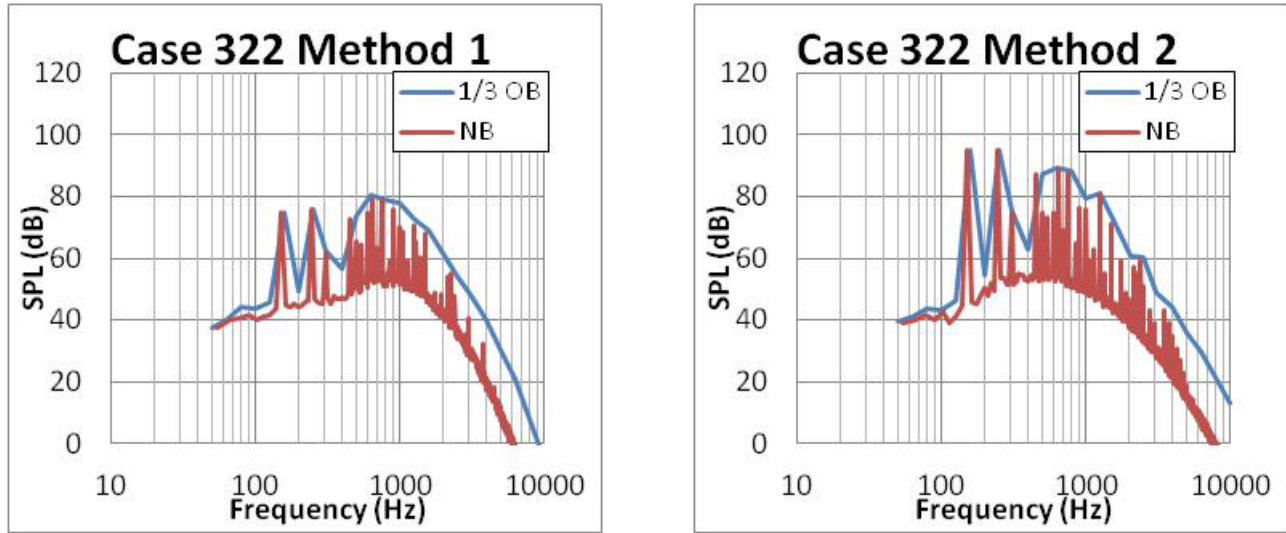
Figure 28: Spectra Comparison for Case 322
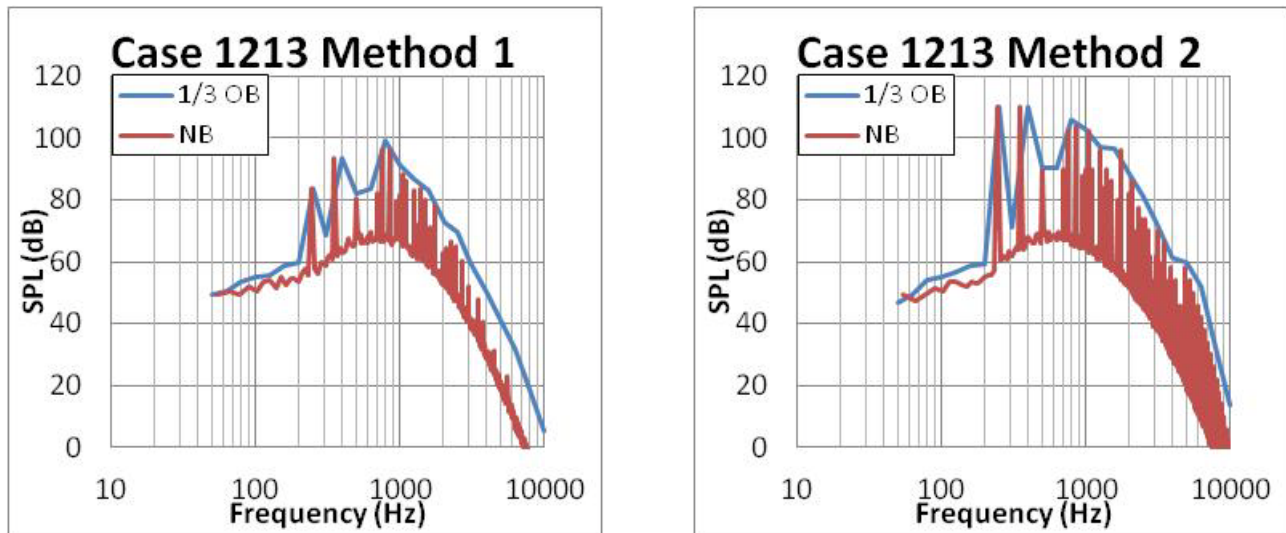
Figure 29: Spectra Comparison for Case 1213

3.1.1 Spectrum Generation Method Comparison

A series of spectra resulting from method 1 and method 2 given the same variable settings (save for tone scalar values) is presented in . The input parameters for each case are presented in Table 2. The method 2 spectra show a dominant primary tone in most cases. Still, for some low TTBB settings, the resulting spectra are predominantly atonal in one-third octave band. Similarly, with high tonal density in the high frequency range, the one-third octave band spectrum appears somewhat atonal. The spectra resulting in relatively atonal one-third octave band spectra due to a lack of narrowband tones (such as Case 2) were excluded from the metric relationship study. However, the atonality in one-third octave band due to high narrowband tonal density was deemed to be a more likely scenario. These cases were included in the metric relationship study.

33

Table 2: Select Spectra DoE Settings

	Run	BBF	BBL	BPFf	BPFa	TTBB	TSf Method 1	TSf Method 2	TSa Method 1	TSa Method 2	TSs Method 1	TSs Method 2
Above Trend Line	80	1000	65	150	150	30	1.5	2	1.5	2	1	2
	797	1000	80	150	150	30	1	1.5	1	1.5	1	2
	2016	400	65	350	150	30	1	1.5	1.5	2	1.5	3
Below Trend Line	2	1000	65	150	150	10	0.5	1	0.5	1	1	2
	322	1000	65	250	150	30	1.5	2	1.5	2	0.5	1
	1213	1000	80	250	350	30	1.5	2	1.5	2	0.5	1

3.1.2 Metric Relationship Results

In the original study, a series of metrics were calculated from the generated spectra, and PNLT was compared to dBA for each spectrum. This process was repeated for the spectra generated from method 2, and the graphs are presented in Figure 30 and Figure 31. The spectra presented in the previous section are highlighted on both PNLT vs. dBA graphs, and the settings for each are reported in Table 2.
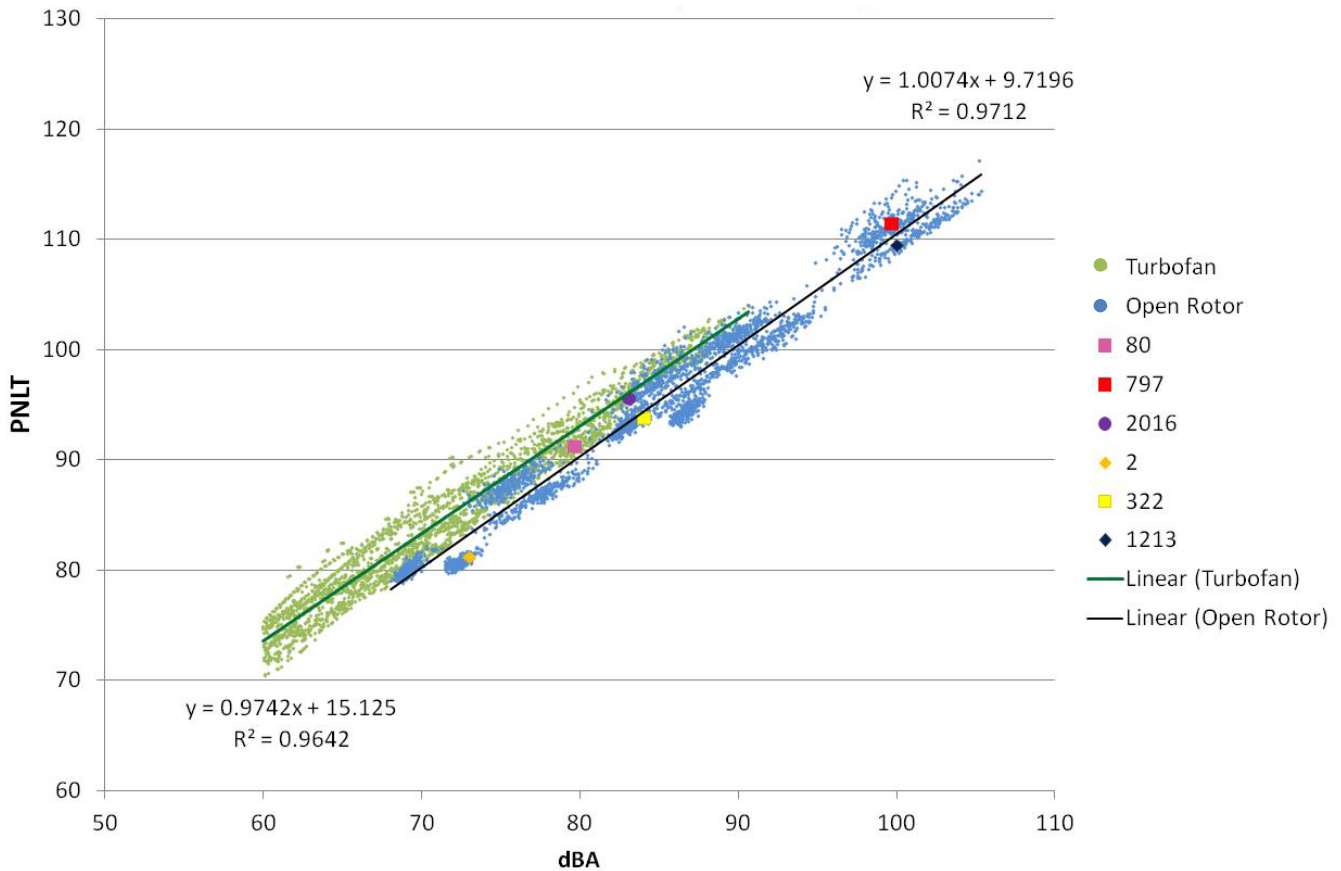
Figure 30: PNLT versus dBA for Method 1

34
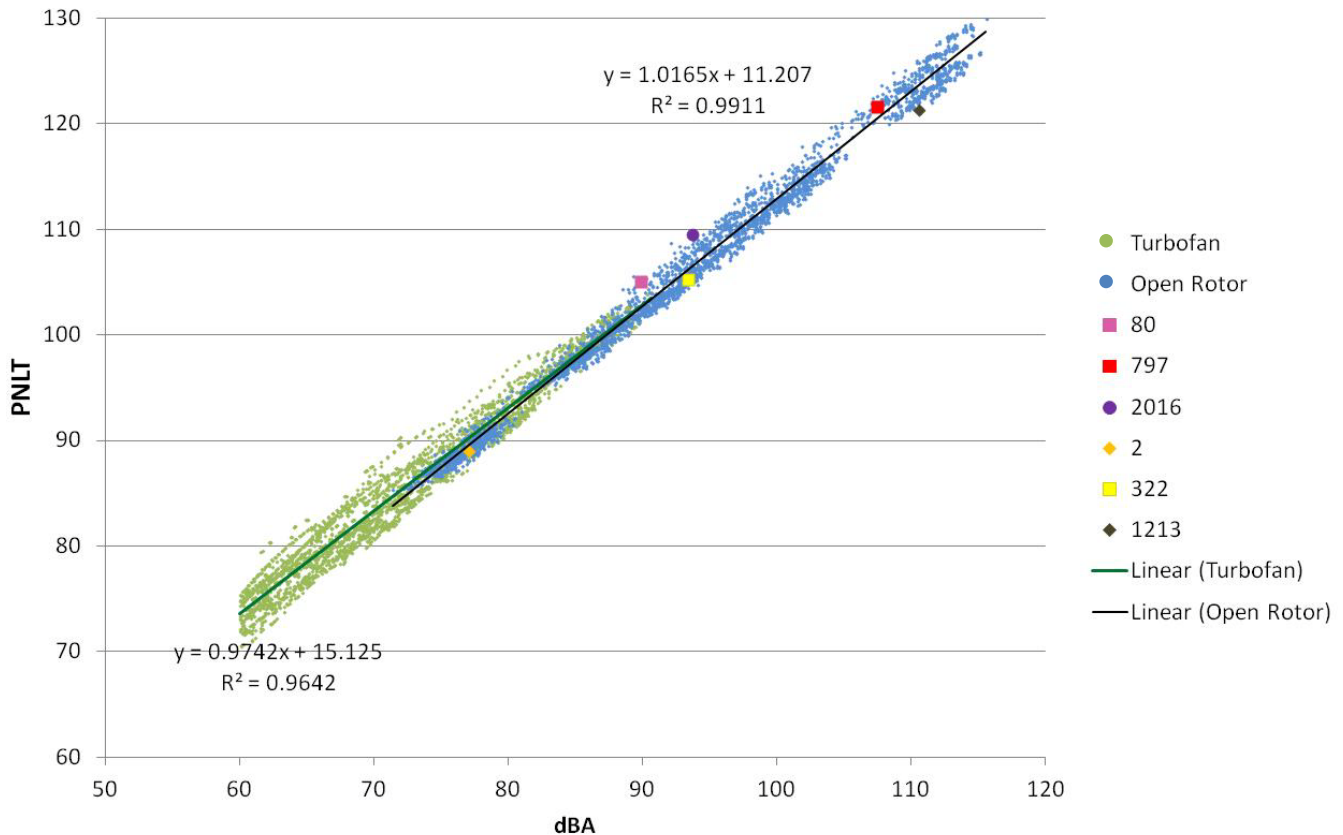
Figure 31: PNLT versus dBA for Method 2

While the graphs of PNLT vs. dBA for the OR cases using method 1 and the TF cases were offset by approximately 2 dB (see Figure 30), the graphs of PNLT vs. dBA for the adjusted OR cases and the TF cases overlapped (see Figure 31). This lead to significantly different conclusions than those reported in the first published paper. This overlap indicated that the relationship between the PNLT and dBA instantaneous metrics was nearly the same for OR and TF cases despite the spectral differences. That is, the certification level to contour area relationship was expected to be similar based solely on instantaneous metrics. That is not to say, however, that some in-flight factors might cause a variation in this relationship. This lead to the efforts in time dependent metric generation for a more in-depth looks into the issue.

4.0 Contour Area Difference

In the generation of a time history and contour, there was no measured data with which to compare our results. The physical expectations along with a comparison of results to the more widely studied and accepted TF case were relied upon to validate the method.

4.1 Physical Expectations

Figure 32 presents a series of received noise spectra at selected time steps corresponding to the positions illustrated in Figure 33. The green spectrum corresponding to the green position marker at 17.5 seconds

illustrates the received noise emitted when the aircraft is almost directly overhead of the observer (marked with the purple position marker). This represents the spectrum most closely matching the stationary, full-power spectrum that was modified for each time step. Directly overhead, there is minimal Doppler shift and directivity attenuation. At this distance, the effects of spherical spreading and atmospheric absorption are minimized. The blue spectrum corresponds to the blue position marker at 0 seconds where the aircraft is moving toward the observer. A Doppler shift to the high frequency can be seen. The attenuation was increased due to the increased distance to the observer relative to the overhead position and thus noise level was decreased. The red spectrum shows the noise received when emitted from the red position marker at 47.5 seconds when the aircraft is moving away from the observer. A Doppler shift to the lower frequency is seen, along with an even higher attenuation relative to the blue position due to the further increased distance to the observer. It is also observed that the high frequency content is more greatly attenuated than the low frequency content due to the higher atmospheric absorption at higher frequencies. The final observation in this plot is the slight change in the shape of the spectra. The green spectrum with very little Doppler shift exhibits wider second and third tones than do the other two spectra. This occurs due to the Doppler shift. The more spread out tones are condensed to the higher or lower frequency bands when shifted. These trends match what is expected and provide confidence in the method.
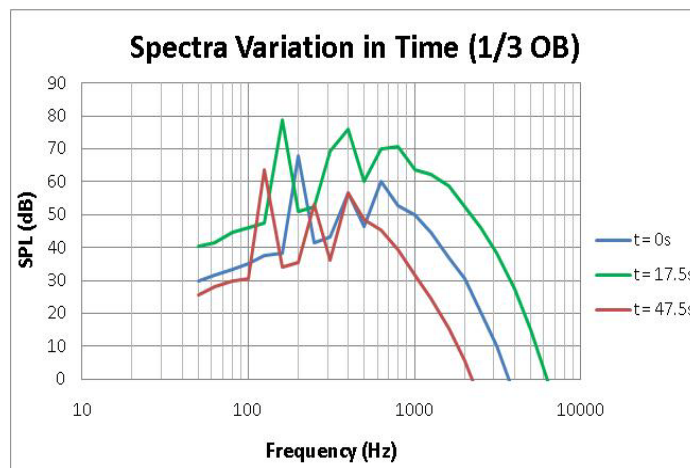
Figure 32: Received Noise Spectra at Selected Time Steps
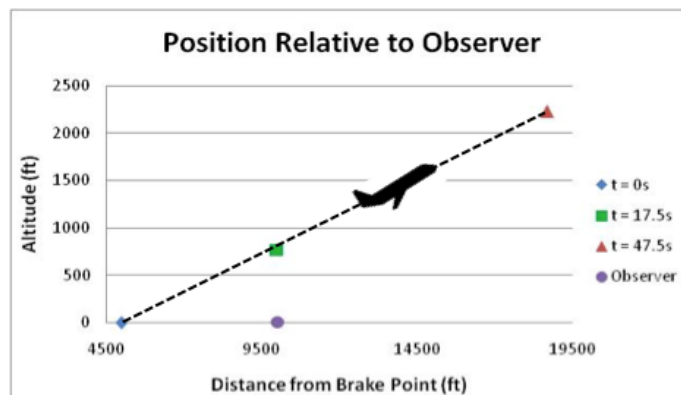
Figure 33: Diagram of Position at Selected Time Steps

36

4.2 ANOPP Comparison

To validate the Georgia Institute of Technology (GT) contour generation method, a TF contour was generated and compared to a TF contour generated using ANOPP. The same TF engine and flight path were used in both methods. The resulting GT contour is presented in Figure 34, and the resulting ANOPP contour is presented in Figure 35. Visual inspection showed a close match. The maximum difference between the noise levels of points farther than 10,000 feet downfield in the direction parallel to the runway was 1.24 dB EPNL and the average difference was 0.48 dB EPNL.
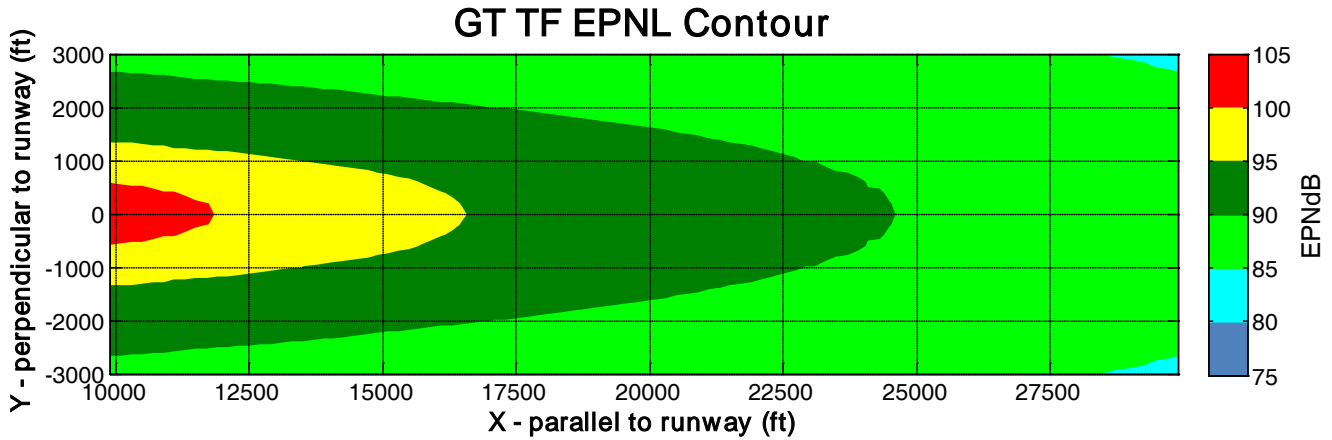
Figure 34: TF EPNL Contour generated with GT method
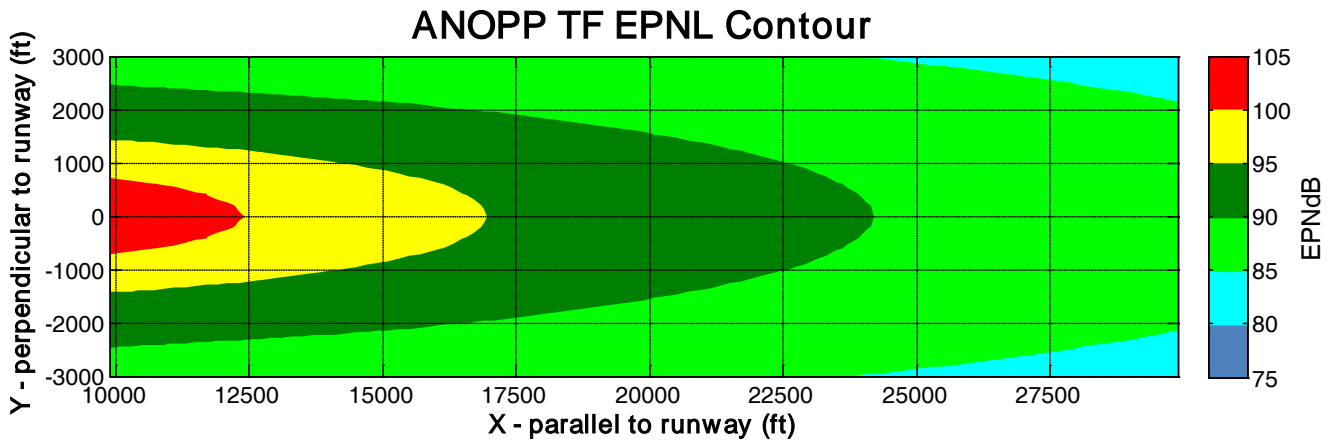
Figure 35: TF EPNL Contour generated with ANOPP

Figure 36 and Figure 37 show SEL contours generated using the GT method and ANOPP respectively. The GT method slightly underestimates the SEL relative to ANOPP with an average of 0.31 SELdB lower calculation for the GT method for observers in the range displayed.
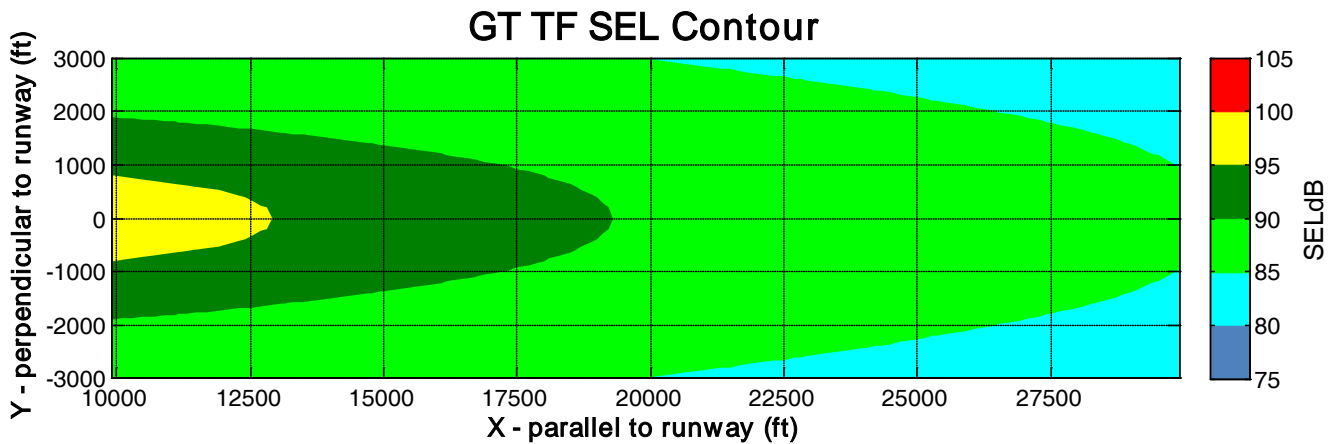
Figure 36: GT TF SEL Contour
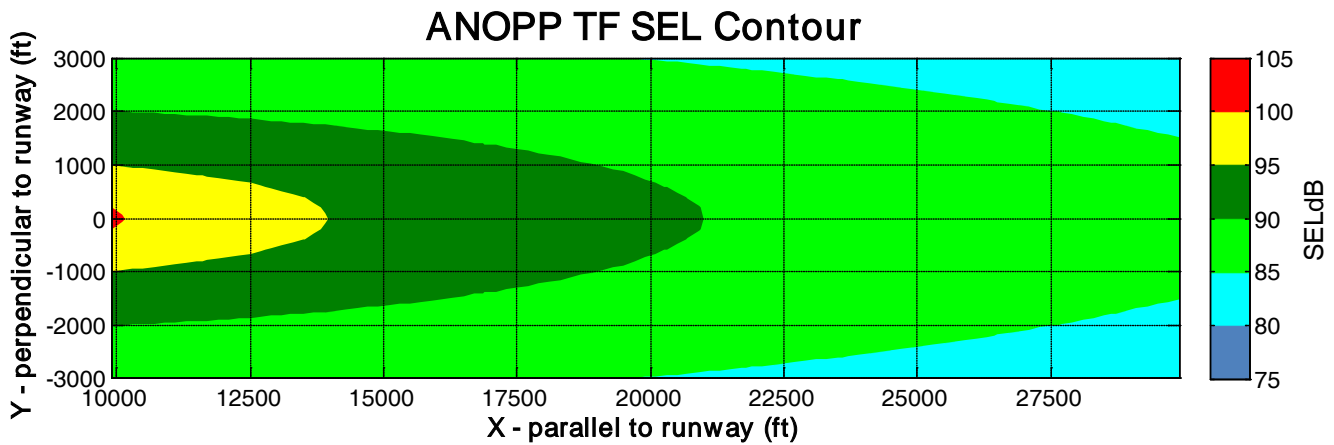
Figure 37: ANOPP TF SEL Contour

5.0 Contour Area Study

To explore the effects of the spectral differences between OR and TF driven aircraft on community noise and the implications of these differences on certification, a study was performed using the tools developed and detailed above to determine the contour area at equal SL certification levels of a wide range of OR cases. A Design of Experiments (DoE) was created to study the effects of variation in design parameters. The target variables included OR spectral variation parameters and flight path parameters. Because of the extensive computing time required for this study, the OR spectral parameters were cut down to include only the range resulting in spectra most closely matching the spectra published by Hoff (1) as seen in Figure 38. The full DoE along with the resulting area differences may be found in Table 4 through Table 9 in the Appendix. For each OR case, the 90 dB EPNL contour area was calculated and compared with the contour area of the TF case validated with the

ANOPP results. The 90 dB EPNL contour area of the TF case was found to be 5.922e7 square feet for all points past 10,000 feet. This value was subtracted from the area of each OR 90 dB EPNL contour to determine the area difference, where a greater contour area difference corresponds to a greater OR contour area.
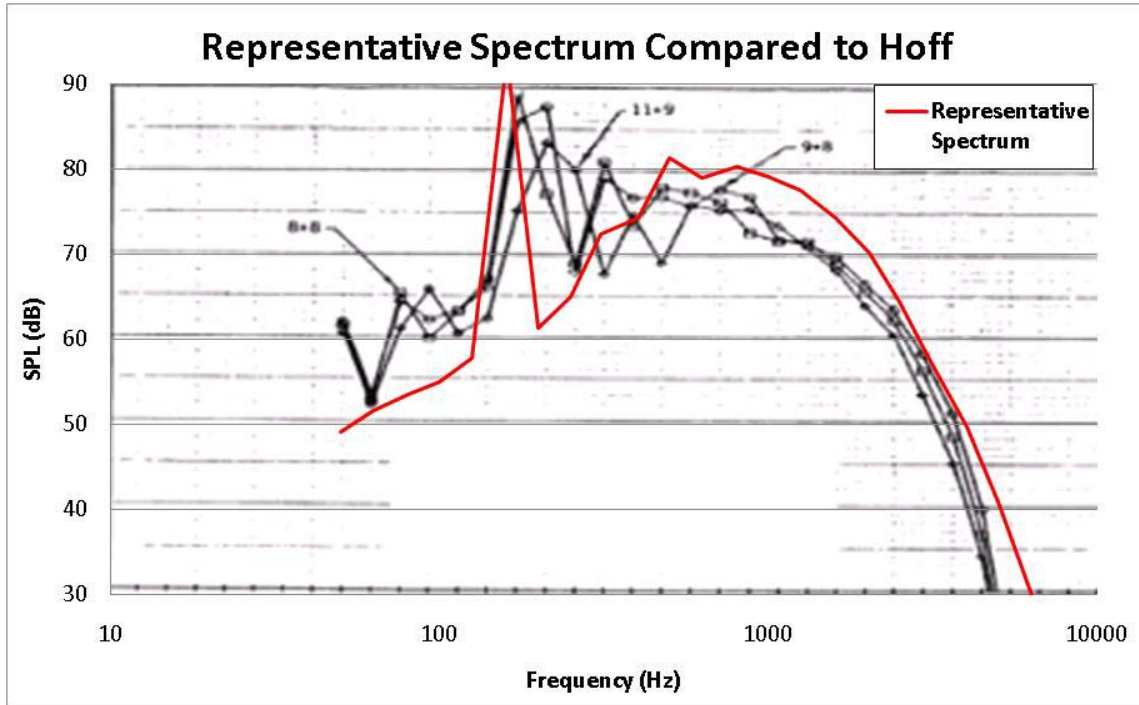
Figure 38: Representative Spectrum Overlaid on Hoff Data

5.1 Contour Comparison

Figure 39 through Figure 42 show select OR EPNL contours with DoE settings presented in Table 3. Figure 43 through Figure 46 show the corresponding SEL contours. The contour variation trends hold for both metrics, but the relative area comparison results do not. Comparing these with the TF contour in Figure 34, it is seen that, for the same SL EPNL, the OR contours have wider minor vertices. The most significant result observed from this study is that for OR and TF driven aircraft at equal SL EPNL, the majority of OR cases result in a greater EPNL contour area. This is especially significant considering the flight paths of the compared contours (seen in Figure 19). However, at the same equal SL EPNL, the SEL contour was on average smaller for the OR than the TF. Because of the excessive tonal content in the OR spectra, the EPNL metric with its tone correction predicts that at equal certification levels, the OR will cause more community annoyance than the TF. The SEL metric with no tonal weighting and reduced weighing of low frequency content predicts that at equal certification levels the TF will cause more community annoyance than the OR.

The climb angle of 96 of the 144 OR cases was greater than that of the TF case. Of these 96 cases, 48 had a 9 degree climb angle and 48 had a 12 degree climb angle compared to the 7.8 degree climb angle of the TF case. All of the cases with 9 degree climb angle exhibited a greater EPNL contour area than

the TF case. Of the 48 cases with a 12 degree climb angle, only 12 resulted in a EPNL contour area less than the TF case.

Table 3: Contour DoE Settings

Case	BBF (Hz)	BBL (dB)	f0f (Hz)	f0a (Hz)	TTBB (dB)	TSf	TSa	TS2	M	theta (deg)	X Vert X (ft)	Y Vert X (ft)	Y Vert Y (ft)	Area Difference (ft^2) EPNL	Area Difference (ft^2) SEL
9	1000	80	150	150	20	1.5	1.5	3	0.25	9	28400	14721	2300	1.15E+07	-4.56E+06
25	1000	80	150	250	20	1.5	1.5	3	0.25	12	23800	13832	2500	-1.40E+06	-7.72E+06
81	400	80	150	150	20	1.5	1.5	3	0.25	9	30400	17376	2400	2.33E+07	-7.64E+06
133	400	80	250	250	20	1.5	1.5	3	0.25	12	24600	13018	2500	1.18E+06	-1.54E+07
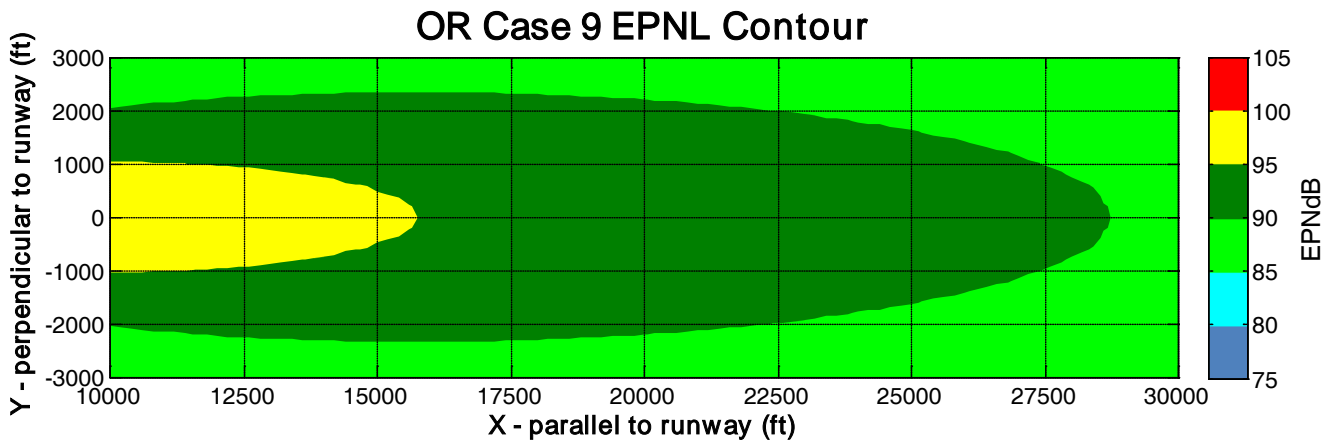
Figure 39: OR Case 9 EPNL Contour
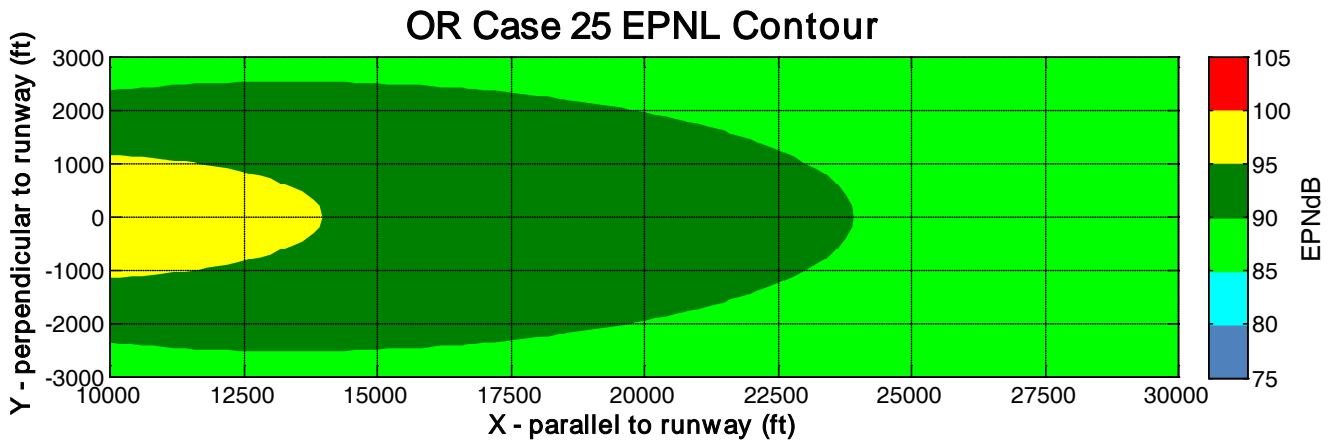
Figure 40: OR Case 25 EPNL Contour
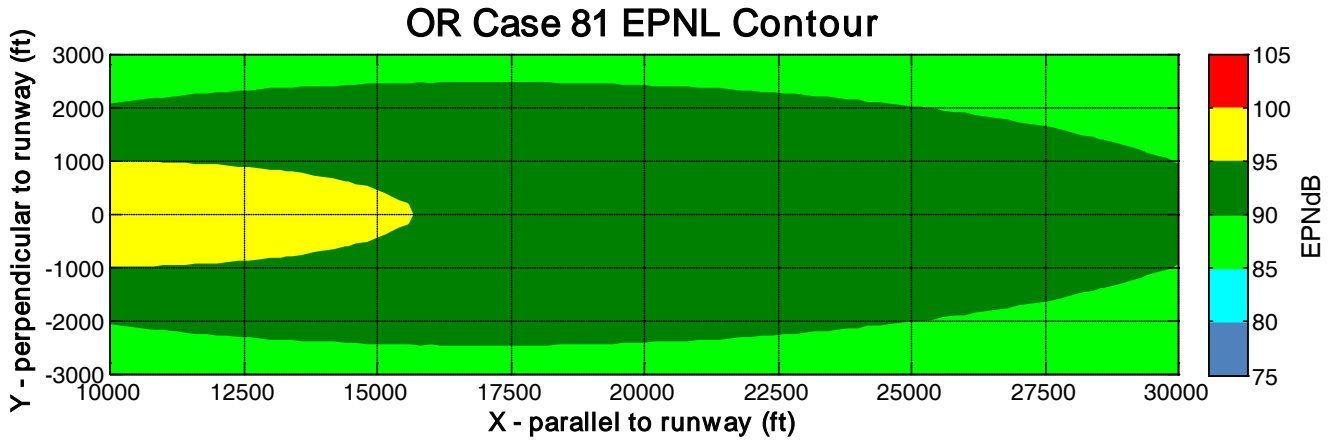
Figure 41: OR Case 81 EPNL Contour
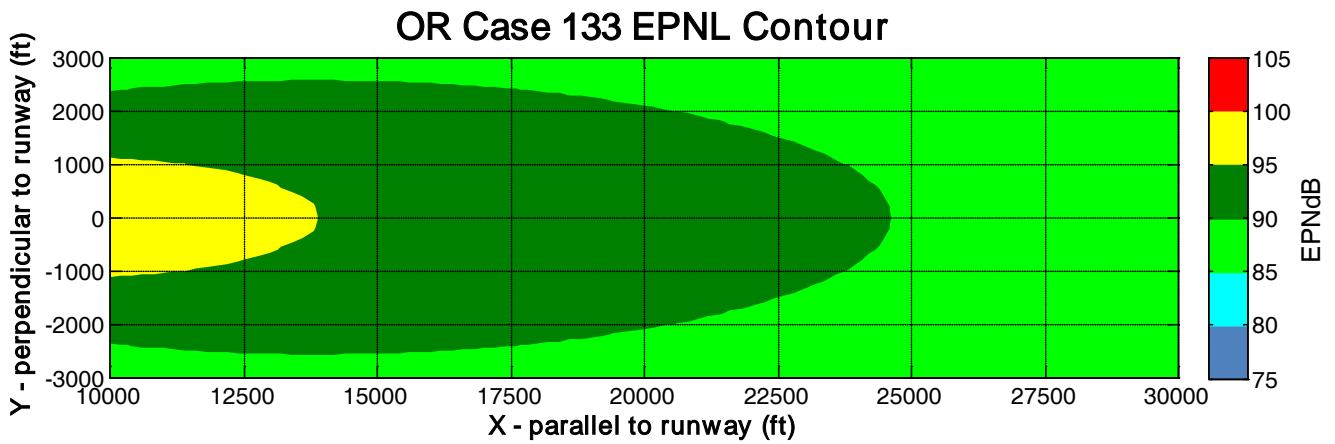
Figure 42: OR Case 133 EPNL Contour
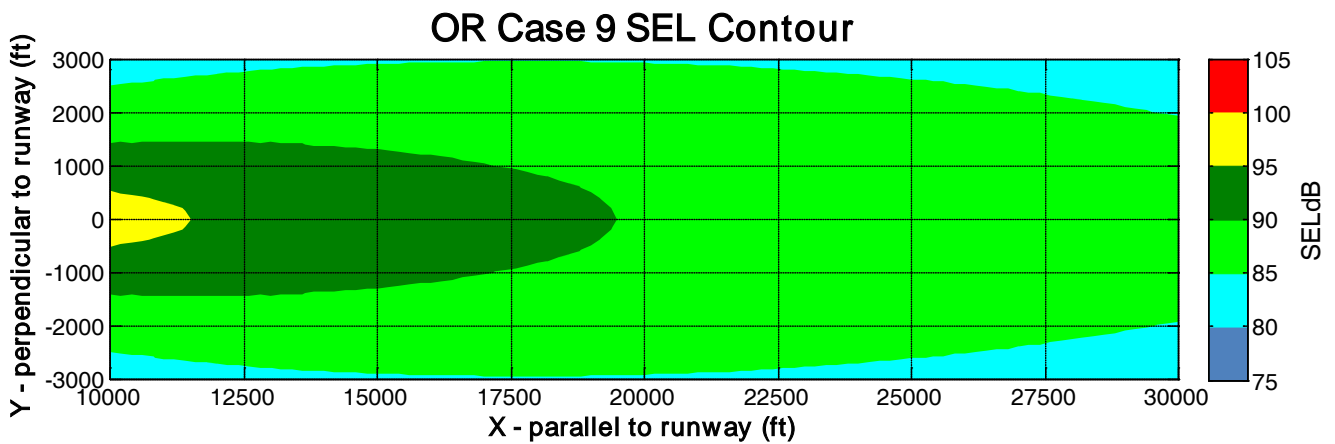
Figure 43: OR Case 9 SEL Contour

41
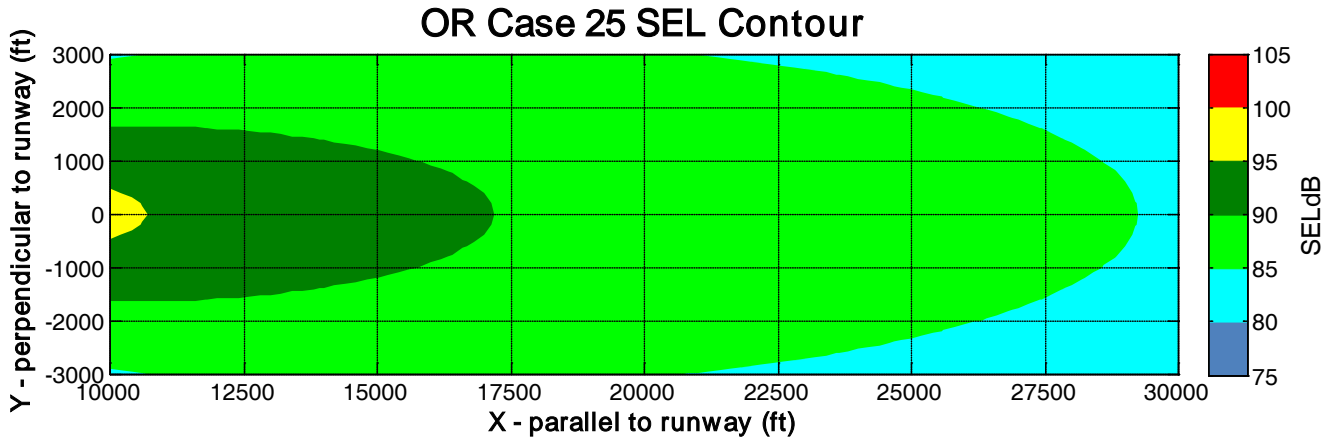
Figure 44: OR Case 25 SEL Contour
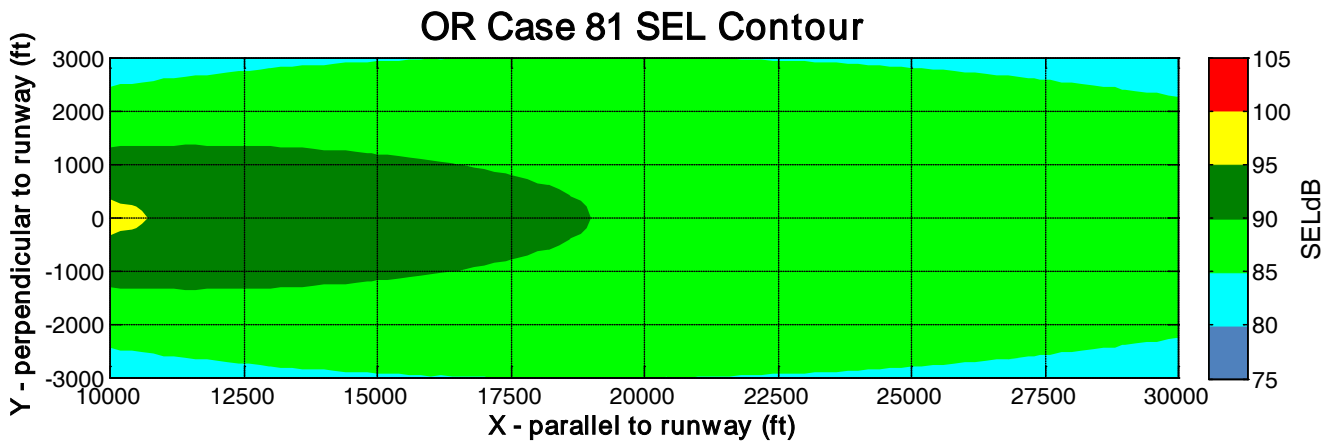
Figure 45: OR Case 81 SEL Contour
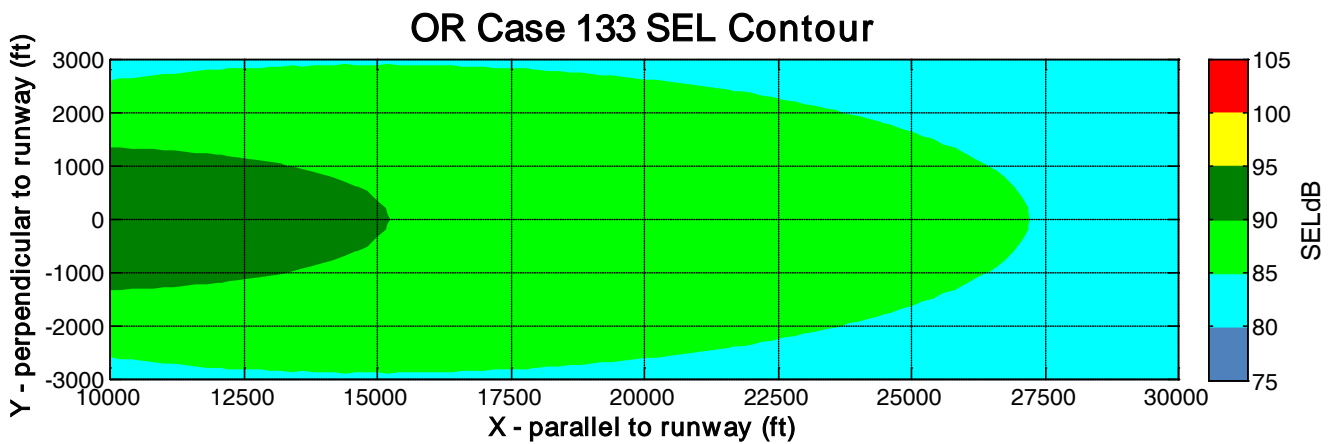
Figure 46: OR Case 133 SEL Contour

5.2 JMP Analysis

Using the program JMP to fit a regression model to the DoE data, variable effects on the contour area were calculated. Figure 52 in the Appendix shows the Prediction Profiler produced by JMP. This series of plots illustrates the effect of each variable setting with the vertical axis of each plot showing the predicted area difference and each horizontal axis showing the level setting of each variable. Thus, a flat line indicates little to no effect of the variable on the area difference, as a large change in the variable results in very little or no change to the area difference. Conversely, a steep line indicates a strong variable effect with a small change in the variable giving rise to a large change in the area difference. The effects of climb angle, Mach number, and BPF are discussed below.

5.2.1 Climb Angle (theta)

The climb angle has the greatest effect on the contour area with the lowest climb angle resulting in the greatest area difference. This result is to be expected as a low climb angle results in a lower altitude, decreasing the distance between source and receiver. The climb angle of the TF case was set at 12 percent (7.8 degrees) landing between the 6 and 9 degree settings of the DoE. Examining the results of the study, the majority of cases resulted in a greater contour area, even when the climb angle of the OR case was less than that of the TF case.

5.2.2 Mach Number (M)

While a low M (and thus increased duration) was expected to result in increased contour area, the results do not reflect this expectation. M has little to no significant effect on the contour area difference. The cause of this unexpected result lies in the level shift of the characteristic spectrum to normalize the SL EPNL, since the EPNL calculation includes a duration correction. By normalizing the SL EPNL, the duration factor is neutralized at the SL observer. Because M is constant throughout the trajectory, the duration factor is neutralized for each observer.

5.2.3 Fore and Aft Blade Passing Frequency (BPFf and BPFa)

While higher BPFs, which result in higher frequency tones, were originally expected to produce greater contour areas than the lower BPFs, this was not observed in the results. Instead, lower BPFs lead to higher contour area difference. Inspection of the spectra received at the observer reveals that the low frequency content dominates the resulting PNLT calculation. Low frequency noise experiences less atmospheric attenuation, and thus travels farther. The high frequency content dominates close to the runway center line. The low frequency tones travel farther than the high frequency tones and contribute greatly to the noise levels farther from the runway. Thus, for two spectra normalized to the SL observer relatively close to the runway center line with one dominated by high frequency content and the other dominated by low frequency content, the spectrum with greater low frequency content will result in a higher EPNL further from the runway center line.

Additionally, the lower frequency BPFs result in a greater number of harmonic tones in the peak annoyance region. These tones contribute to a peak in the high annoyance region that is higher than that of the higher BPFs for all distances from the runway center line.

To illustrate these phenomena, Figure 47 and Figure 48 were generated. Figure 47 shows two received spectra in a trajectory at different distances (d_1 and d_2) propagated from the same characteristic spectrum with $BPF_f = BPF_a = BPF = 150$ Hz and $d_1 < d_2$. Figure 48 shows two received spectra at the same distances as the spectra in Figure 47 propagated from the same characteristic spectrum with $BPF_f = BPF_a = BPF = 350$ Hz. The 2nd and 3rd tones in the 350 Hz BPF graph are significantly more attenuated than those in the 150 Hz BPF graph. Though less visible, the first tone in the 350 Hz BPF graph is attenuated by about 1 dB more than the first tone in the 150 Hz BPF graph showing a significant reduction in acoustic energy. Additionally, because the first tone in the 350 Hz BPF case contributes more annoyance at short distances than the first tone in the 150 Hz BPF case, the overall level was more highly attenuated to result in the same normalized SL EPNL. Thus, the tones in the high annoyance range were concurrently more highly attenuated in the 350 Hz BPF case than in the 150 Hz BPF case.
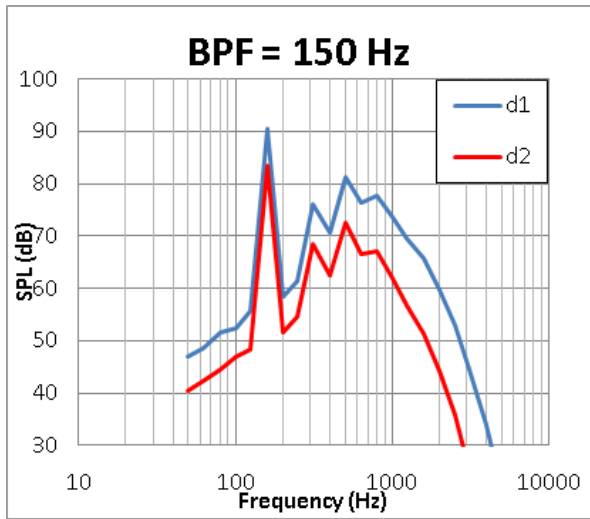
Figure 47: 150 Hz BPF Tone Attenuation Illustration
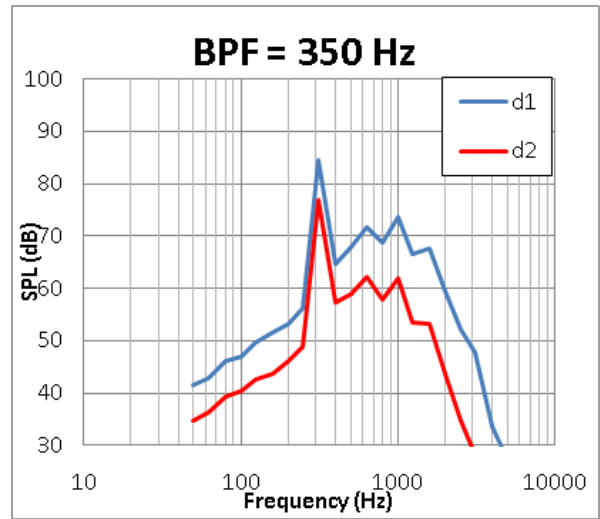
Figure 48: 350 Hz BPF Tone Attenuation Illustration

5.3 Spectral Analysis

To investigate the cause of the increased contour area for the OR cases, the received noise spectra were examined and compared to those produced by the TF case. Figure 49 through Figure 51 show the received spectra resulting in maximum PNLT for the SL observer of several OR cases compared to the maximum PNLT spectrum of the TF case for the same observer. For each OR case, the maximum PNLT (presented in the graph titles) was greater than that of the TF case. The first tone of each OR spectrum is approximately 10 dB higher than the TF level of the given frequency neighborhood. Subsequent OR spectra tones in the peak annoyance range also have significantly higher level than the TF spectra. It was determined that the extended propagation of the low frequency tones of the OR

44

spectra contributed to greater EPNL at further distances from the emission point leading to increased contour area.
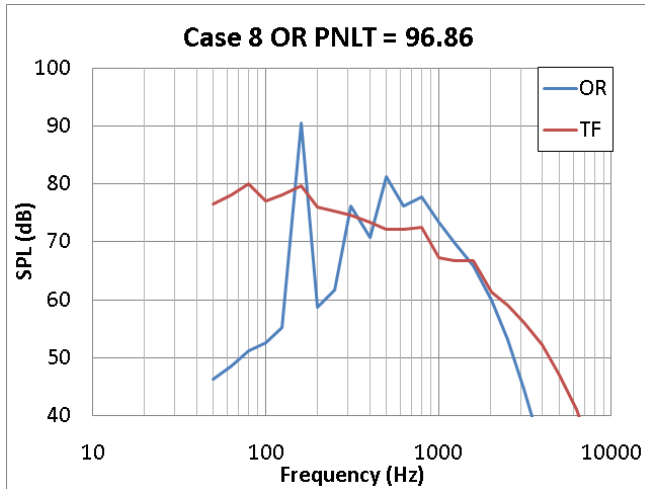
Figure 49: OR Case 8 Max PNLT Spectrum Comparison
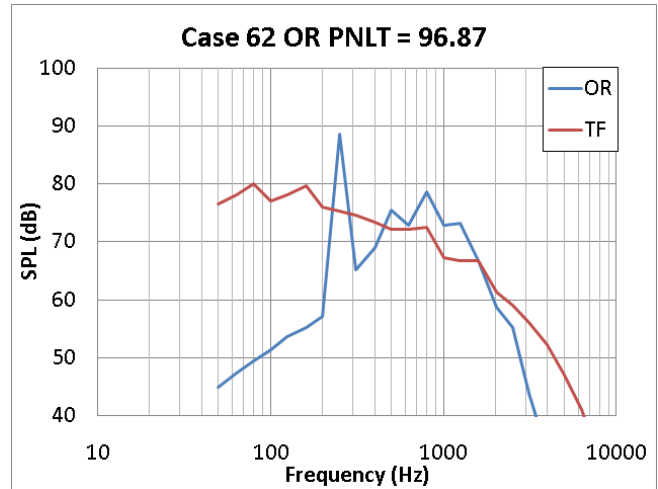
Figure 50: OR Case 62 Max PNLT Spectrum Comparison
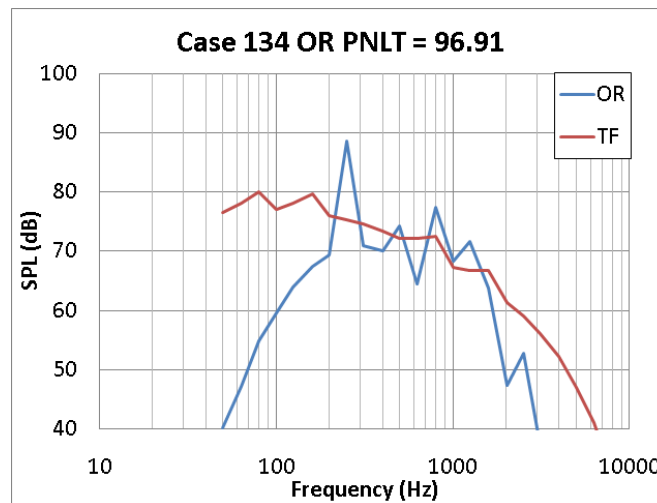
Figure 51: OR Case 134 Max PNLT Spectrum Comparison

6.0 Conclusion

By leveraging the work performed in the first year of Project 35, the parametric generation of representative OR spectra was extended to generate noise contours representing the noise produced by an OR driven aircraft exhibiting a noise spectrum comparable to the range of representative spectra produced. By applying propagation effects to characteristic spectra through parametrically generated flight paths, time histories of noise received at stationary observer positions were calculated. Contours were produced by generating a time history of received noise for a grid of stationary observers. This method was validated through the contour generation of a 300 passenger class TF driven aircraft and comparison of that contour with ANOPP EPNL calculations for the same aircraft and observer grid.

Approximating the contour shape as an ellipse, the lengths of the major and minor vertices were determined using optimization techniques to find the area of the 90 dB EPNL. The levels of the characteristic OR spectra were normalized to result in an equal SL EPNL to that of the 300 passenger class TF case. A DoE was generated to determine design variable effects on the 90 dB EPNL contour area of 144 OR cases. Comparing this to the 90 dB EPNL contour of the 300 passenger class TF case used for validation provided the area difference.

This study resulted in following:

1. The study performed showed a clear trend of greater contour area for the OR cases relative to that of the TF case at equal SL EPNL. This trend held even for OR cases with flight paths having a greater climb angle than that of the TF case. Through examination of the data, it was determined that this trend was caused by the increased low frequency spectral content of the OR cases. Because low frequency sound is attenuated less by atmospheric absorption than high frequency sound, the low frequency content in the OR spectra propagated farther and resulted in higher EPNL at greater distances from the flight path.
2. JMP analysis results.
3. The climb angle has the greatest effect on the contour area with the lowest climb angle resulting in the greatest area difference. At smaller climb angle, the aircraft climbs more slowly passing closer to observers further downfield. This resulted in increased levels further down field and subsequently greater contour area.
4. M has little to no significant effect on the contour area difference. The normalization of the spectrum level to result in an equal SL EPNL led to this misleading result.
5. Lower BPFs lead to higher contour area difference. Inspection of the spectra received at the observer reveals that the low frequency content dominates the resulting PNLT calculation. …..
6. For each OR case, the maximum PNLT (presented in the graph titles) was greater than that of the TF case. It was determined that the extended propagation of the low frequency tones of the OR spectra contributed to greater EPNL at further distances from the emission point leading to increased contour area.

Author's recommendations for a future work:

1. While the second iteration of the OR spectrum generation tool is a noted improvement, there is still room for progress in the method to more closely match the Hoff data (Hoff 1990). A TTBB value for both fore and aft blade rows would provide more flexibility.
2. In addition, inclusion of more measured OR acoustic data would provide a better base for the investigation.
3. OR design has changed much since the Hoff data was published, so updated measured data would also serve to allow for better representation of the likely attributes of OR noise.
4. A fleet level assessment may be performed to model various fleet insertion scenarios to compare the insertion of OR-powered aircraft with TF aircraft of comparable ERA.

7.0 References

1. «ANOPP Theoretical Manual.» T. Noise Levels Module LEV. NASA, February 2008 r. 6.1.1-6.1.11.

2. «GPO Access, Electronic Code and Federal Regulations.» *FAR 36 Appendix A.* 15 January 2010 r. http://ecfr.gpoaccess.gov/cgi/t/text/text-idx?type=simple;c=ecfr;cc=ecfr;sid=1146aa176c1a84276602015ab1ebca70;idno=14;region=DIV1;q1=a36.4;rgn=div9;view=text;node=14%3A1.0.1.3.19.10.363.4.44 (дата обращения: 15 January 2010 r.).

3. Hastings, Aaron. *Program to Calculate Loudness Based on DIN 45631.* MATLAB M-file. Herrick Labs, Purdue University. 31 October 2000 r.

4. Hoff, G. E. et al. *Experimental Performance and Acoustic Investigation of Modern, Counterrotating Blade Concepts.* NASA Contractor Report 185158, Cincinatti: GE Aircraft Engines, 1990.

5. Kinsler, Lawrence E, Austin R Frey, Alen B Coppens, и James V Sanders. *Fundamental of Acoustics.* Fourth. John Wiley and Sons, Inc., 1999.

6. McCurdy, David A, и Robert E Grandle. *Aircraft Noise Synthesis System.* NASA, Hampton, VA: NASA Langley Research Center, 1987.

7. McCurdy, David A. *Annoyancy Caused by Advanced Turboprop Aircraft Flyover Noise, Counter-Rotating Propeller Configuration.* NASA Technical Paper 3027, Hampton, Virginia: NASA Langley Research Center, 1990.

8. Powell, C. A. *Relationship between Aircraft Noise Contour Area and Noise Levels at Certification Points.* NASA, 2003.

9. Stevens, S.S. «Procedure for Calculating Loudness: Mark VI.» *The Journal of the Acoustical Society of America* 33, № 11 (November 1961): 1577-1585.

10. Vanderplaats, G. *Multidiscipline Design Optimization.* Monterey, CA: Vanderplaats Research and Development Inc., 2007.

11. Young, R, J Tai, B Havrilesko, и D Mavris. «A Comparison of Community Noise Metrics for Open Rotor Engine Architectures.» *16th AIAA/CEAS Aeroacoustics Conference.* Stockholm: AIAA, 2010.

12. Zwicker, E. et al. «BASIC program for calculating the loudness of sounds from their 1/3 oct band spectra accoring to ISO 532 B.» *Acoustica* 55 (1948): 63-67.

8.0 Appendix

Table 4: Contour Area Study DoE (1-35)

Case	BBF (Hz)	BBL (dB)	f0f (Hz)	f0a (Hz)	TTBB (dB)	TSf	TSa	TS2	M	theta (deg)	X Vert X (ft)	Y Vert X (ft)	Y (ft)	Area Difference (ft^2) EPNL	SEL
1	1000	80	150	150	20	1.5	1.5	3	0.15	12	24600	13181	2500	1.32E+06	-1.04E+07
2	1000	80	150	150	20	1.5	1.5	3	0.15	6	37400	20557	2200	4.22E+07	1.24E+07
3	1000	80	150	150	20	1.5	1.5	3	0.15	9	28800	15774	2300	1.35E+07	-3.89E+06
4	1000	80	150	150	20	1.5	1.5	3	0.2	12	24600	14033	2500	1.94E+06	-8.16E+06
5	1000	80	150	150	20	1.5	1.5	3	0.2	6	37400	20132	2200	4.23E+07	1.12E+07
6	1000	80	150	150	20	1.5	1.5	3	0.2	9	28800	15147	2300	1.32E+07	-4.65E+06
7	1000	80	150	150	20	1.5	1.5	3	0.25	12	24200	13018	2500	-4.03E+05	-8.22E+06
8	1000	80	150	150	20	1.5	1.5	3	0.25	6	37400	20557	2200	4.22E+07	1.12E+07
9	1000	80	150	150	20	1.5	1.5	3	0.25	9	28400	14721	2300	1.15E+07	-4.56E+06
10	1000	80	150	150	30	1.5	1.5	3	0.15	12	25200	13970	2500	4.31E+06	-1.93E+07
11	1000	80	150	150	30	1.5	1.5	3	0.15	6	37800	20395	2300	4.85E+07	-7.43E+06
12	1000	80	150	150	30	1.5	1.5	3	0.15	9	30200	16362	2400	2.24E+07	-1.67E+07
13	1000	80	150	150	30	1.5	1.5	3	0.2	12	25400	14721	2600	8.12E+06	-1.95E+07
14	1000	80	150	150	30	1.5	1.5	3	0.2	6	38000	23475	2400	4.90E+07	-7.50E+06
15	1000	80	150	150	30	1.5	1.5	3	0.2	9	30000	16525	2400	2.16E+07	-1.67E+07
16	1000	80	150	150	30	1.5	1.5	3	0.25	12	25200	14033	2500	4.35E+06	-1.92E+07
17	1000	80	150	150	30	1.5	1.5	3	0.25	6	37800	22361	2300	4.66E+07	-8.00E+06
18	1000	80	150	150	30	1.5	1.5	3	0.25	9	29800	15635	2300	1.72E+07	-1.65E+07
19	1000	80	150	250	20	1.5	1.5	3	0.15	12	23800	13282	2500	-1.78E+06	-7.44E+06
20	1000	80	150	250	20	1.5	1.5	3	0.15	6	37200	20820	2200	4.13E+07	1.33E+07
21	1000	80	150	250	20	1.5	1.5	3	0.15	9	28000	15248	2300	1.03E+07	-1.79E+06
22	1000	80	150	250	20	1.5	1.5	3	0.2	12	23800	14071	2500	-1.27E+06	-7.65E+06
23	1000	80	150	250	20	1.5	1.5	3	0.2	6	37200	20557	2200	4.14E+07	1.29E+07
24	1000	80	150	250	20	1.5	1.5	3	0.2	9	27800	15472	2300	9.64E+06	-4.21E+06
25	1000	80	150	250	20	1.5	1.5	3	0.25	12	23800	13832	2500	-1.40E+06	-7.72E+06
26	1000	80	150	250	20	1.5	1.5	3	0.25	6	37000	20132	2200	4.08E+07	1.16E+07
27	1000	80	150	250	20	1.5	1.5	3	0.25	9	28000	14884	2300	1.01E+07	-2.42E+06
28	1000	80	150	250	30	1.5	1.5	3	0.15	12	24200	13181	2500	-2.66E+05	-6.81E+06
29	1000	80	150	250	30	1.5	1.5	3	0.15	6	37400	21246	2200	4.17E+07	1.51E+07
30	1000	80	150	250	30	1.5	1.5	3	0.15	9	28800	15147	2300	1.32E+07	-8.69E+05
31	1000	80	150	250	30	1.5	1.5	3	0.2	12	24400	13506	2500	7.84E+05	-6.67E+06
32	1000	80	150	250	30	1.5	1.5	3	0.2	6	37600	20132	2300	4.77E+07	1.47E+07
33	1000	80	150	250	30	1.5	1.5	3	0.2	9	28200	15472	2300	1.11E+07	-6.43E+05
34	1000	80	150	250	30	1.5	1.5	3	0.25	12	24400	13018	2500	3.89E+05	-6.72E+06
35	1000	80	150	250	30	1.5	1.5	3	0.25	6	37400	20557	2200	4.22E+07	1.39E+07

Table 5: Contour Area Study DoE (36-70)

Case	BBF (Hz)	BBL (dB)	f0f (Hz)	f0a (Hz)	TTBB (dB)	TSf	TSa	TS2	M	theta (deg)	X Vert X (ft)	Y Vert X (ft)	Y (ft)	Area Difference (ft^2) EPNL	SEL
36	1000	80	150	250	30	1.5	1.5	3	0.25	9	28200	14721	2300	1.07E+07	-4.68E+05
37	1000	80	250	150	20	1.5	1.5	3	0.15	12	24000	13282	2500	-9.80E+05	-7.61E+06
38	1000	80	250	150	20	1.5	1.5	3	0.15	6	37200	21246	2200	4.09E+07	1.33E+07
39	1000	80	250	150	20	1.5	1.5	3	0.15	9	28000	15248	2300	1.03E+07	-3.45E+06
40	1000	80	250	150	20	1.5	1.5	3	0.2	12	24000	14071	2500	-4.59E+05	-7.68E+06
41	1000	80	250	150	20	1.5	1.5	3	0.2	6	37200	20557	2200	4.14E+07	1.29E+07
42	1000	80	250	150	20	1.5	1.5	3	0.2	9	27800	15472	2200	6.64E+06	-4.21E+06
43	1000	80	250	150	20	1.5	1.5	3	0.25	12	23800	13832	2500	-1.40E+06	-7.72E+06
44	1000	80	250	150	20	1.5	1.5	3	0.25	6	37200	20132	2200	4.16E+07	1.16E+07
45	1000	80	250	150	20	1.5	1.5	3	0.25	9	28000	14884	2300	1.01E+07	-4.12E+06
46	1000	80	250	150	30	1.5	1.5	3	0.15	12	24200	13870	2500	2.34E+05	-1.50E+07
47	1000	80	250	150	30	1.5	1.5	3	0.15	6	37600	21246	2300	4.72E+07	1.28E+06
48	1000	80	250	150	30	1.5	1.5	3	0.15	9	28800	16362	2300	1.37E+07	-1.10E+07
49	1000	80	250	150	30	1.5	1.5	3	0.2	12	24600	13506	2500	1.58E+06	-1.46E+07
50	1000	80	250	150	30	1.5	1.5	3	0.2	6	37600	20820	2300	4.75E+07	2.46E+06
51	1000	80	250	150	30	1.5	1.5	3	0.2	9	28600	16099	2300	1.28E+07	-1.11E+07
52	1000	80	250	150	30	1.5	1.5	3	0.25	12	24600	14033	2600	4.39E+06	-1.45E+07
53	1000	80	250	150	30	1.5	1.5	3	0.25	6	37600	20557	2300	4.76E+07	8.56E+05
54	1000	80	250	150	30	1.5	1.5	3	0.25	9	28600	14721	2300	1.22E+07	-1.13E+07
55	1000	80	250	250	20	1.5	1.5	3	0.15	12	24000	13282	2500	-9.80E+05	-8.44E+06
56	1000	80	250	250	20	1.5	1.5	3	0.15	6	37200	21246	2200	4.09E+07	1.24E+07
57	1000	80	250	250	20	1.5	1.5	3	0.15	9	27600	15147	2200	5.80E+06	-4.34E+06
58	1000	80	250	250	20	1.5	1.5	3	0.2	12	23800	13607	2500	-1.54E+06	-8.16E+06
59	1000	80	250	250	20	1.5	1.5	3	0.2	6	37200	20557	2200	4.14E+07	1.24E+07
60	1000	80	250	250	20	1.5	1.5	3	0.2	9	27800	15472	2200	6.64E+06	-4.65E+06
61	1000	80	250	250	20	1.5	1.5	3	0.25	12	23800	13506	2500	-1.61E+06	-8.22E+06
62	1000	80	250	250	20	1.5	1.5	3	0.25	6	37200	20557	2200	4.14E+07	1.07E+07
63	1000	80	250	250	20	1.5	1.5	3	0.25	9	28000	14884	2300	1.01E+07	-4.89E+06
64	1000	80	250	250	30	1.5	1.5	3	0.15	12	24400	13181	2500	5.27E+05	-9.92E+06
65	1000	80	250	250	30	1.5	1.5	3	0.15	6	37600	20557	2300	4.76E+07	1.24E+07
66	1000	80	250	250	30	1.5	1.5	3	0.15	9	28400	15774	2300	1.20E+07	-4.78E+06
67	1000	80	250	250	30	1.5	1.5	3	0.2	12	24200	14033	2500	3.30E+05	-1.01E+07
68	1000	80	250	250	30	1.5	1.5	3	0.2	6	37400	20132	2200	4.23E+07	1.20E+07
69	1000	80	250	250	30	1.5	1.5	3	0.2	9	28400	15147	2300	1.17E+07	-5.05E+06
70	1000	80	250	250	30	1.5	1.5	3	0.25	12	24600	14033	2600	4.39E+06	-1.00E+07

Table 6: Contour Area Study DoE (71-110)

Case	BBF (Hz)	BBL (dB)	f0f (Hz)	f0a (Hz)	TTBB (dB)	TSf	TSa	TS2	M	theta (deg)	X Vert X (ft)	Y Vert X (ft)	Y (ft)	Area Difference (ft^2) EPNL	SEL
76	400	80	150	150	20	1.5	1.5	3	0.2	12	26200	14721	2600	1.15E+07	-1.23E+07
77	400	80	150	150	20	1.5	1.5	3	0.2	6	38000	23475	2400	4.90E+07	7.43E+06
78	400	80	150	150	20	1.5	1.5	3	0.2	9	30600	17639	2400	2.41E+07	-7.42E+06
79	400	80	150	150	20	1.5	1.5	3	0.25	12	26000	15673	2600	1.09E+07	-1.20E+07
80	400	80	150	150	20	1.5	1.5	3	0.25	6	38000	22098	2400	5.26E+07	6.50E+06
81	400	80	150	150	20	1.5	1.5	3	0.25	9	30400	17376	2400	2.33E+07	-7.64E+06
82	400	80	150	150	30	1.5	1.5	3	0.15	12	25800	15147	2600	9.97E+06	-1.70E+07
83	400	80	150	150	30	1.5	1.5	3	0.15	6	38000	22724	2400	5.14E+07	-2.38E+06
84	400	80	150	150	30	1.5	1.5	3	0.15	9	30400	17113	2400	2.33E+07	-1.17E+07
85	400	80	150	150	30	1.5	1.5	3	0.2	12	26200	14721	2600	1.15E+07	-1.70E+07
86	400	80	150	150	30	1.5	1.5	3	0.2	6	38000	23212	2400	5.00E+07	-1.42E+06
87	400	80	150	150	30	1.5	1.5	3	0.2	9	30400	17902	2400	2.31E+07	-1.36E+07
88	400	80	150	150	30	1.5	1.5	3	0.25	12	26400	14884	2700	1.52E+07	-1.66E+07
89	400	80	150	150	30	1.5	1.5	3	0.25	6	38000	22198	2400	5.24E+07	-2.70E+06
90	400	80	150	150	30	1.5	1.5	3	0.25	9	30800	17376	2400	2.49E+07	-1.38E+07
91	400	80	150	250	20	1.5	1.5	3	0.15	12	24400	13870	2500	1.04E+06	-1.09E+07
92	400	80	150	250	20	1.5	1.5	3	0.15	6	37600	21246	2300	4.72E+07	8.72E+06
93	400	80	150	250	20	1.5	1.5	3	0.15	9	29200	16362	2300	1.52E+07	-7.23E+06
94	400	80	150	250	20	1.5	1.5	3	0.2	12	24600	13506	2500	1.58E+06	-1.06E+07
95	400	80	150	250	20	1.5	1.5	3	0.2	6	37600	20557	2300	4.76E+07	8.66E+06
96	400	80	150	250	20	1.5	1.5	3	0.2	9	29200	16099	2300	1.51E+07	-7.23E+06
97	400	80	150	250	20	1.5	1.5	3	0.25	12	24800	14033	2600	5.22E+06	-1.10E+07
98	400	80	150	250	20	1.5	1.5	3	0.25	6	37400	20557	2200	4.22E+07	7.76E+06
99	400	80	150	250	20	1.5	1.5	3	0.25	9	28800	16262	2300	1.36E+07	-7.14E+06
100	400	80	150	250	30	1.5	1.5	3	0.15	12	24600	13870	2500	1.84E+06	-6.81E+06
101	400	80	150	250	30	1.5	1.5	3	0.15	6	37400	20557	2300	4.68E+07	1.34E+07
102	400	80	150	250	30	1.5	1.5	3	0.15	9	28800	16362	2300	1.37E+07	-3.89E+06
103	400	80	150	250	30	1.5	1.5	3	0.2	12	24600	13506	2500	1.58E+06	-8.18E+06
104	400	80	150	250	30	1.5	1.5	3	0.2	6	37600	20132	2200	4.31E+07	1.34E+07
105	400	80	150	250	30	1.5	1.5	3	0.2	9	29000	16099	2300	1.44E+07	-2.80E+06
106	400	80	150	250	30	1.5	1.5	3	0.25	12	24400	13018	2500	3.89E+05	-7.72E+06
107	400	80	150	250	30	1.5	1.5	3	0.25	6	37600	20557	2300	4.76E+07	1.30E+07
108	400	80	150	250	30	1.5	1.5	3	0.25	9	28600	14721	2300	1.22E+07	-3.51E+06
109	400	80	250	150	20	1.5	1.5	3	0.15	12	24600	13870	2500	1.84E+06	-1.32E+07
110	400	80	250	150	20	1.5	1.5	3	0.15	6	37600	21246	2300	4.72E+07	2.87E+06

Table 7: Contour Area Study DoE (111-144)

Case	BBF (Hz)	BBL (dB)	f0f (Hz)	f0a (Hz)	TTBB (dB)	TSf	TSa	TS2	M	theta (deg)	X Vert X (ft)	Y Vert X (ft)	Y Vert Y (ft)	Area Difference (ft^2) EPNL	Area Difference (ft^2) SEL
111	400	80	250	150	20	1.5	1.5	3	0.15	9	29000	16362	2300	1.44E+07	-8.45E+06
112	400	80	250	150	20	1.5	1.5	3	0.2	12	25000	14296	2600	6.22E+06	-1.28E+07
113	400	80	250	150	20	1.5	1.5	3	0.2	6	37800	20720	2300	4.83E+07	2.86E+06
114	400	80	250	150	20	1.5	1.5	3	0.2	9	29200	16099	2300	1.51E+07	-1.00E+07
115	400	80	250	150	20	1.5	1.5	3	0.25	12	24800	14033	2500	2.75E+06	-1.33E+07
116	400	80	250	150	20	1.5	1.5	3	0.25	6	37600	20557	2300	4.76E+07	3.21E+06
117	400	80	250	150	20	1.5	1.5	3	0.25	9	29400	14721	2300	1.51E+07	-1.02E+07
118	400	80	250	150	30	1.5	1.5	3	0.15	12	24800	13970	2600	5.18E+06	-1.54E+07
119	400	80	250	150	30	1.5	1.5	3	0.15	6	37600	21246	2300	4.72E+07	-1.33E+06
120	400	80	250	150	30	1.5	1.5	3	0.15	9	29000	16362	2300	1.44E+07	-1.13E+07
121	400	80	250	150	30	1.5	1.5	3	0.2	12	24800	13506	2500	2.38E+06	-1.50E+07
122	400	80	250	150	30	1.5	1.5	3	0.2	6	37800	20720	2300	4.83E+07	-2.12E+06
123	400	80	250	150	30	1.5	1.5	3	0.2	9	29000	16099	2300	1.44E+07	-1.33E+07
124	400	80	250	150	30	1.5	1.5	3	0.25	12	24800	14033	2600	5.22E+06	-1.54E+07
125	400	80	250	150	30	1.5	1.5	3	0.25	6	37600	20557	2300	4.76E+07	-2.35E+06
126	400	80	250	150	30	1.5	1.5	3	0.25	9	29400	14884	2300	1.53E+07	-1.13E+07
127	400	80	250	250	20	1.5	1.5	3	0.15	12	24600	13181	2500	1.32E+06	-1.58E+07
128	400	80	250	250	20	1.5	1.5	3	0.15	6	37600	20557	2300	4.76E+07	8.41E+05
129	400	80	250	250	20	1.5	1.5	3	0.15	9	29000	15774	2300	1.43E+07	-1.17E+07
130	400	80	250	250	20	1.5	1.5	3	0.2	12	24400	13506	2500	7.84E+05	-1.55E+07
131	400	80	250	250	20	1.5	1.5	3	0.2	6	37600	20132	2300	4.77E+07	8.78E+05
132	400	80	250	250	20	1.5	1.5	3	0.2	9	29000	15999	2300	1.43E+07	-1.21E+07
133	400	80	250	250	20	1.5	1.5	3	0.25	12	24600	13018	2500	1.18E+06	-1.54E+07
134	400	80	250	250	20	1.5	1.5	3	0.25	6	37600	20557	2300	4.76E+07	-2.74E+06
135	400	80	250	250	20	1.5	1.5	3	0.25	9	29000	14721	2300	1.37E+07	-1.16E+07
136	400	80	250	250	30	1.5	1.5	3	0.15	12	24600	13181	2500	1.32E+06	-1.93E+07
137	400	80	250	250	30	1.5	1.5	3	0.15	6	37400	21246	2200	4.17E+07	-7.20E+06
138	400	80	250	250	30	1.5	1.5	3	0.15	9	28400	15147	2300	1.17E+07	-1.67E+07
139	400	80	250	250	30	1.5	1.5	3	0.2	12	24200	13506	2500	-1.31E+04	-1.95E+07
140	400	80	250	250	30	1.5	1.5	3	0.2	6	37600	20820	2300	4.75E+07	-7.50E+06
141	400	80	250	250	30	1.5	1.5	3	0.2	9	28600	15472	2300	1.26E+07	-1.68E+07
142	400	80	250	250	30	1.5	1.5	3	0.25	12	24600	14033	2600	4.39E+06	-1.92E+07
143	400	80	250	250	30	1.5	1.5	3	0.25	6	37400	20557	2200	4.22E+07	-8.03E+06
144	400	80	250	250	30	1.5	1.5	3	0.25	9	28600	14721	2300	1.22E+07	-1.69E+07

Table 8:

| Steady Loading Tones						Interaction tones		
Tone Number	Relative Attenuation	Tone Number	Relative Attenuation	Tone Number	Relative Attenuation	Forward Multiple	Aft Multiple	Relative Attenuation
1	0	45	−88	89	−176	1	0	0
2	−10	46	−90	90	−178	0	1	−2
3	−4	47	−92	91	−180	1	1	−15
4	−10	48	−94	92	−182	2	1	−11
5	−7	49	−96	93	−184	1	2	−3
6	−12	50	−98	94	−186	3	1	−13
7	−18	51	−100	95	−188	2	2	−28
8	−24	52	−102	96	−190	1	3	−10
9	−20	53	−104	97	−192	4	1	−15
10	−22	54	−106	98	−194	3	2	−30
11	−26	55	−108	99	−196	2	3	−32
12	−28	56	−110	100	−198	1	4	−18
13	−32	57	−112	101	−200	5	1	−14
14	−26	58	−114	102	−202	1	5	−25
15	−28	59	−116	103	−204	6	1	−17
16	−30	60	−118	104	−206	1	6	−33
17	−32	61	−120	105	−208	7	1	−20
18	−34	62	−122	106	−210	1	7	−23
19	−36	63	−124	107	−212	8	1	−24
20	−38	64	−126	108	−214	1	8	−19
21	−40	65	−128	109	−216	9	1	−25
22	−42	66	−130	110	−218	1	9	−18
23	−44	67	−132	111	−220			
24	−46	68	−134	112	−222			
25	−48	69	−136	113	−224			
26	−50	70	−138	114	−226			
27	−52	71	−140	115	−228			
28	−54	72	−142	116	−230			
29	−56	73	−144	117	−232			
30	−58	74	−146	118	−234			
31	−60	75	−148	119	−236			
32	−62	76	−150	120	−238			
33	−64	77	−152	121	−240			
34	−66	78	−154	122	−242			
35	−68	79	−156	123	−244			
36	−70	80	−158	124	−246			
37	−72	81	−160	125	−248			
38	−74	82	−162	126	−250			
39	−76	83	−164					
40	−78	84	−166					
41	−80	85	−168					
42	−82	86	−170					
43	−84	87	−172					
44	−86	88	−174					
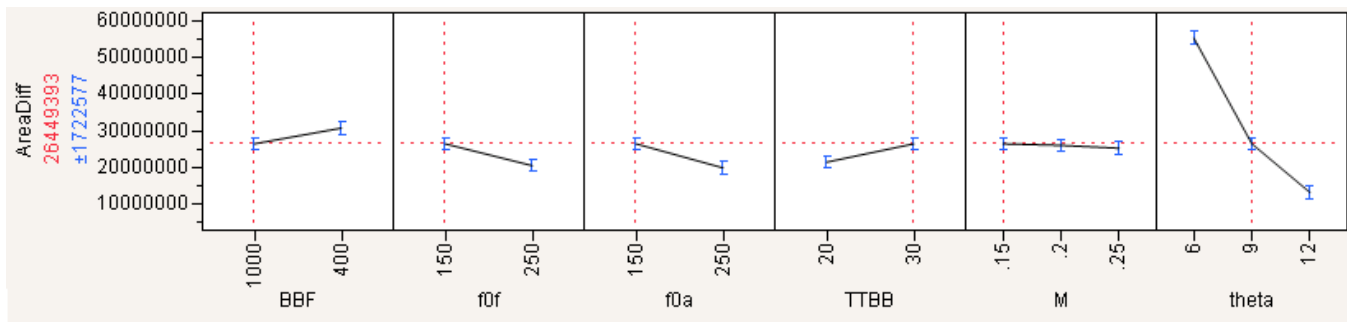
Figure 52: JMP Prediction Profiler